27
6-5-78
25 NTIS

ORNL/NUREG/TM-194

Heavy-Section Steel Technology Program Quarterly Progress Report for October–December 1977

G. D. Whitman
R. H. Bryan

Prepared for the U.S. Nuclear Regulatory Commission
Office of Nuclear Regulatory Research
Under Interagency Agreements DOE 40-551-75 and 40-552-75

MASTER

OAK RIDGE NATIONAL LABORATORY

OPERATED BY UNION CARBIDE CORPORATION · FOR THE DEPARTMENT OF ENERGY

Printed in the United States of America. Available from
National Technical Information Service
U.S. Department of Commerce
5285 Port Royal Road, Springfield, Virginia 22161
Price: Printed Copy $6.00; Microfiche $3.00

ORNL/NUREG/TM-194
Dist. Category NRC-5

Contract No. W-7405-eng-26

Engineering Technology Division

HEAVY-SECTION STEEL TECHNOLOGY PROGRAM QUARTERLY PROGRESS REPORT FOR OCTOBER–DECEMBER 1977

G. D. Whitman R. H. Bryan

Manuscript Completed — April 12, 1978
Date Published — May 1978

NOTICE: This document contains information of a preliminary nature. It is subject to revision or correction and therefore does not represent a final report.

Prepared for the
U.S. Nuclear Regulatory Commission
Office of Nuclear Regulatory Research
Under Interagency Agreements DOE 40-551-75 and 40-552-75

Prepared by the
OAK RIDGE NATIONAL LABORATORY
Oak Ridge, Tennessee 37830
operated by
UNION CARBIDE CORPORATION
for the
DEPARTMENT OF ENERGY

CONTENTS

PREFACE

The Heavy-Section Steel Technology (HSST) Program, which is sponsored by the Nuclear Regulatory Commission (NRC), is an engineering research activity devoted to extending and developing the technology for assessing the margin of safety against fracture of the thick-walled steel pressure vessels used in light-water-cooled nuclear power reactors. The program is being carried out in close cooperation with the nuclear power industry. This report covers HSST work performed October through December 1977, except for subcontractor contributions which may cover the three-month period ending in November. The work performed by Oak Ridge National Laboratory (ORNL) and by subcontractors is managed by the Engineering Technology Division. Major tasks at ORNL are carried out by the Engineering Technology Division and the Metals and Ceramics Division. Prior progress reports on this program are ORNL-4176, ORNL-4315, ORNL-4377, ORNL-4463, ORNL-4512, ORNL-4590, ORNL-4653, ORNL-4681, ORNL-4764, ORNL-4816, ORNL-4855, ORNL-4918, ORNL-4971, ORNL-4655 (Vol. II), ORNL/TM-4729 (Vol. II), ORNL/TM-4805 (Vol. II), ORNL/TM-4914 (Vol. II), ORNL/TM-5021 (Vol. II), ORNL/TM-5170, ORNL/NUREG/TM-3, ORNL/NUREG/TM-28, ORNL/NUREG/TM-49, ORNL/NUREG/TM-64, ORNL/NUREG/TM-94, ORNL/NUREG/TM-120, ORNL/NUREG/TM-147, and ORNL/NUREG/TM-166.

SUMMARY*

1. PROGRAM ADMINISTRATION AND PROCUREMENT

The Heavy-Section Steel Technology (HSST) Program is an engineering research activity conducted by the Oak Ridge National Laboratory (ORNL) for the Nuclear Regulatory Commission (NRC) in coordination with other research sponsored by the federal government and private organizations. The program comprises studies relating to all areas of the technology of the materials fabricated into thick-section primary-coolant containment systems of light-water-cooled nuclear power reactors. The principal area of investigation is the behavior and structural integrity of steel pressure vessels containing cracklike flaws. Current work is organized into the following tasks: (1) program administration, (2) fracture mechanics analyses and investigations, (3) effect of high-temperature primary reactor water on the subcritical crack growth of reactor vessel steel, (4) investigations of irradiated materials, (5) pressure vessel investigations, (6) thermal shock investigations, and (7) foreign research.

The work performed under the 4 existing research and development subcontracts is included in this report.

During this quarter 19 program briefings or presentations were made.

2. FRACTURE MECHANICS ANALYSES AND INVESTIGATIONS

Stress-intensity factor distributions along the tip of nozzle corner cracks in models of intermediate test vessels (ITVs) and boiling-water reactor (BWR) vessels have been measured by photoelastic techniques. The measurements in the ITV models agree reasonably well with the results of burst tests performed earlier in the HSST program. Comparison of BWR model values with results of analytical studies also indicates agreement except for shallow flaws. Stress-intensity factors for shallow flaws may be lower than predicted because the analytical flaw shapes are not realistic for flaws within the fillet region.

---

*Conversions from SI to English units for all SI quantities are listed on a foldout page at the end of this report.

3. EFFECT OF HIGH-TEMPERATURE PRIMARY REACTOR WATER ON THE SUBCRITICAL CRACK GROWTH OF REACTOR VESSEL STEEL

Testing of specimens of submerged-arc weld material was completed. Crack growth rates observed in the last specimen compare well with previous results of tests of weld material. These welds appear to be more resistant to crack propagation than base metal.

The testing of one specimen was completed in the study of the effects of ramp and hold time on crack growth rates. Initial crack growth was consistent with previous data, but experimental problems prevented clear conclusions from the latter part of the test.

Examination of fracture surfaces of fatigue specimens of weld metal, A533B, and A508 class 2 indicates that the mechanism of crack propagation in weld metal is different from that of base material in a PWR environment. In this environment crack propagation occurs in base material by ductile striation formation and in weld metal by void coalescence.

4. INVESTIGATIONS OF IRRADIATED MATERIALS

During this period, 74 Charpy V-notch specimens from the second 4T-CTS irradiation experiment were tested. The tests show radiation-induced increases of the temperatures of Charpy energy transition and onset upper-shelf energy at irradiative temperatures as high as 345°C. Upper-shelf energy and lateral expansion were diminished by irradiation.

Multiple-specimen techniques using 10-mm-thick compact specimens were applied to determine the J_{Ic} of irradiated A533-B1, and a J_{Ic} value of 155 kJ/m^2 was obtained.

A program for evaluating the unloading compliance technique of single-specimen J-integral testing was developed. Evaluation and improvement of equipment were initiated.

5. PRESSURE VESSEL INVESTIGATIONS

The procedures and equipment for preparing the flaw in intermediate test vessel V-8 were tried on a cylindrical remnant of vessel V-9. The

equipment functioned properly, and the resulting prototypic fatigue-sharpened flaw was satisfactory.

Continuing studies of fracture toughness in preparation for the V-8 test involved submerged-arc weld metal from the V-9 prolongation, half-bead repair weld metal from a qualification test plate, and submerged-arc weld metal from the V-8 prolongation near the prototypic repair weld. Compact specimens 51 mm thick from the V-9 weld were tested. These are the largest specimens tested for weld metal in the vessels fabricated from steel plate. Fractographic examination of fractured precracked Charpy V-notch specimens from V-8 indicates that, in the apparent transition temperature regime, the high and low values of K_{Icd} are associated with two distinct weld metal structures; specimens precracked in reaustenitized sections of a weld pass exhibit ductile fracture, while specimens precracked in columnar structures within a weld pass fracture frangibly.

Further fracture toughness tests of materials used in the crack-arrest model tests were performed.

6. THERMAL SHOCK INVESTIGATIONS

A liquid-nitrogen facility for thermal shock testing 533-mm-OD cylinders was constructed and run with water and liquid nitrogen. A new method for applying a coating that enhances heat transfer to the liquid nitrogen was developed and evaluated with small-scale specimens.

7. FOREIGN RESEARCH

Lists of foreign reports published in *Nuclear Safety* through Vol. 19 (No. 1) have been reviewed to identify topics of interest in the metallurgy and materials areas. Translated copies of reports of interest have been requested, and translations received are being reviewed.

HEAVY-SECTION STEEL TECHNOLOGY PROGRAM QUARTERLY PROGRESS REPORT FOR OCTOBER–DECEMBER 1977

G. D. Whitman R. H. Bryan

ABSTRACT

The Heavy-Section Steel Technology (HSST) Program is an engineering research activity conducted by the Oak Ridge National Laboratory for the Nuclear Regulatory Commission. It comprises studies related to all areas of the technology of the materials fabricated into thick-section primary-coolant containment systems of light-water-cooled nuclear power reactors. The principal area of investigation is the behavior and structural integrity of steel pressure vessels containing cracklike flaws. Current work is organized into seven tasks: (1) program administration and procurement, (2) fracture mechanics analyses and investigations, (3) effect of high-temperature primary reactor water on subcritical crack growth, (4) investigations of irradiated materials, (5) pressure vessel investigations, (6) thermal shock investigations, and (7) foreign research.

The stress-intensity factors measured photoelastically for nozzle corner cracks compare well with calculated values except for shallow flaws, in which case results may be sensitive to differences in crack shape. Fatigue testing of weld metal was completed, and ramp- and hold-time studies of forging material continue. Charpy specimens of irradiated weld metal with low ductile shelf toughness were tested, and other preparations for J-integral testing of larger specimens of this material were made. Procedures and equipment for flawing vessel V-8 were demonstrated to be satisfactory, and material properties of this vessel were studied. A facility for performing thermal shock experiments with liquid nitrogen was completed. Studies of enhanced heat transfer from coated cylinders continued.

1. PROGRAM ADMINISTRATION AND PROCUREMENT

G. D. Whitman

The Heavy-Section Steel Technology (HSST) Program, a major safety program sponsored by the Nuclear Regulatory Commission (NRC), is concerned with the structural integrity of the primary systems, particularly the reactor pressure vessels of light-water-cooled nuclear power reactor stations. The structural integrity of these vessels is ensured by

designing and fabricating them according to the standards set by the code for nuclear pressure vessels, by detecting flaws of significant size that occur during fabrication and in service, and by developing methods capable of producing quantitative estimates of conditions under which fractures could occur. The program is concerned mainly with developing pertinent fracture technology. It deals with the development of knowledge of the material used in these thick-walled vessels, the rate of growth of flaws, and the combination of flaw size and load that would cause fracture and thus limit the life and/or operating conditions for this reactor plant.

The program is coordinated with other government agencies and the manufacturing and utility sectors of the nuclear power industry in the United States and abroad. The overall objective is a quantification of safety assessments for regulatory agencies, professional code-writing bodies, and the nuclear power industry. Several of the activities are conducted under subcontracts by research facilities in the United States and through informal cooperative efforts on an international basis. Four research and development subcontracts are currently in force.

Administratively, the program is organized into seven tasks, as reflected in this report: (1) program administration and procurement, (2) fracture mechanics analyses and investigations, (3) effect of high-temperature primary water on subcritical crack growth of reactor vessel steel, (4) investigations of irradiated material, (5) pressure vessel investigations, (6) thermal shock investigations, and (7) foreign research.

During this quarter, 19 program briefings, reviews, or presentations were made by the HSST staff at technical meetings and at program reviews for the NRC staff or for visitors.

2. FRACTURE MECHANICS ANALYSES AND INVESTIGATIONS*

2.1 Stress Intensity Factors for Nozzle Cracks in Reactor Vessels†

C. W. Smith†† W. H. Peters††

2.1.1 Introduction

Stress-intensity factor (SIF) determination for cracks emanating from the juncture of reactor vessels with inlet and exit nozzles has been a problem in the reactor vessel industry for many years due to the complex and widely varying geometries involved. To date, only approximate analytical solutions such as those of Hellen and Dowling,[1] Reynen,[2] Broekhoven and Spaas,[3] and Schmitt et al.[4] are available in the open literature, but substantial additional efforts are also under way.

As a result of the degree of analytical intractability of the problem and the need for experimental correlation of approximate analytical methods such as the finite-element method (FEM), the authors have undertaken several experimental investigations. The experimental technique employed[5-12] has been developed by the authors over a period of years and consists of a marriage between the "frozen stress" photoelastic analysis of cracked bodies with a simplified digital computer analysis of the experimental data for extracting the SIF.

This study has consisted of two phases to date. The first phase consisted in applying the above technique to a cracked nozzle geometry identical to that studied by Derby[13] approximating that of an intermediate

---

*Conversions from SI to English units for all SI quantities are listed on a foldout page at the end of this report.

†Research performed by the Photoelasticity and Fracture Laboratory in the Engineering Science and Mechanics Dept. at Virginia Polytechnic Institute and State University under Subcontract No. 7015 between Union Carbide Corporation and Virginia Polytechnic Institute and State University.

††Engineering Science and Mechanics Dept., Virginia Polytechnic Institute and State University.

test vessel (ITV). Details of the first phase of the study are found in Ref. 14.

After comparison with the Derby residual static strength technique, the study entered phase II, which involved frozen stress photoelastic determination of SIF distributions for a scale model of a cracked inlet nozzle for an existing boiling-water reactor vessel (BWR) with cracks oriented normal to the vessel hoop stress as in phase I (Fig. 2.1). After briefly reviewing the analytical basis of the technique, the results of phases I and II will be noted and compared with other studies. (Part of the results of phase II is found in Ref. 15). Progress on phase III of the study, where cracks are initiated at different locations around the nozzle periphery (Fig. 2.1), will also be briefly described.

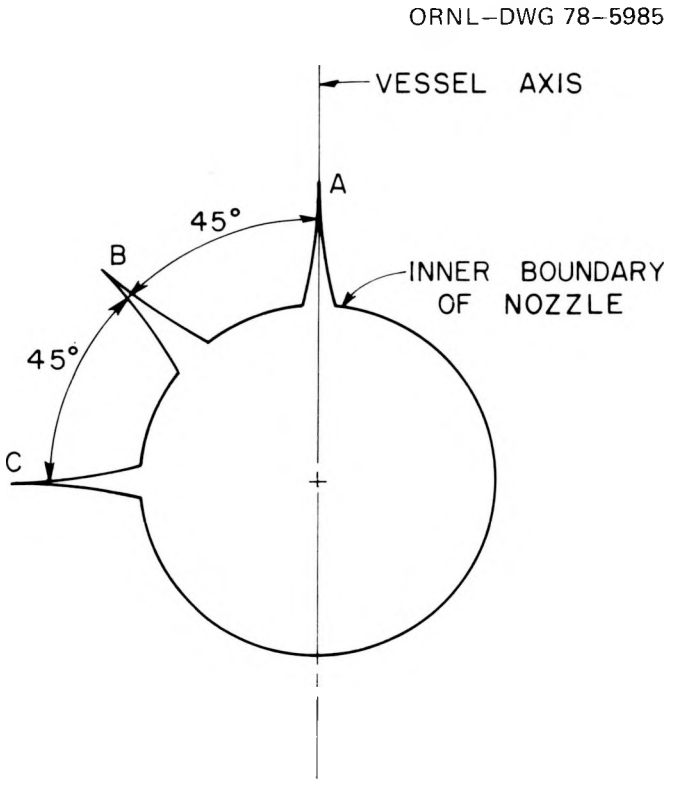

Fig. 2.1. Crack orientations relative to vessel axis (A, phases I and II; B and C, phase III).

2.1.2 Analytical considerations

One can express the maximum shearing stress in the nz plane along $\theta = \pi/2$ (Fig. 2.2) near the crack tip in the form[9]

$$\tau_{max} = \frac{A}{r^{1/2}} + B \ , \tag{1}$$

where $A = K_I/(8\pi)^{1/2}$, K_I = SIF, and B is the leading term of a Taylor Series expansion of the regular stress field near the crack tip. Data are taken along $\theta = \pi/2$ since fringes tend to spread in that direction (Fig. 2.3). Then, from the Stress Optic Law,

$$\tau_{max} = \frac{Nf}{2t} \ , \tag{2}$$

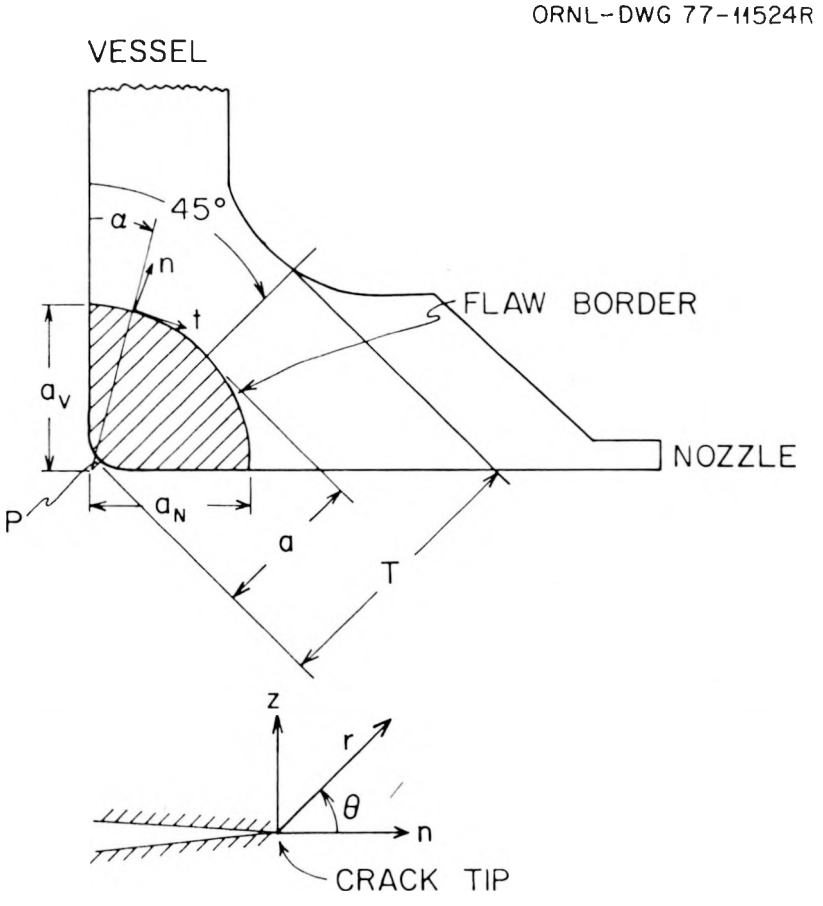

Fig. 2.2. Local problem geometry and notation.

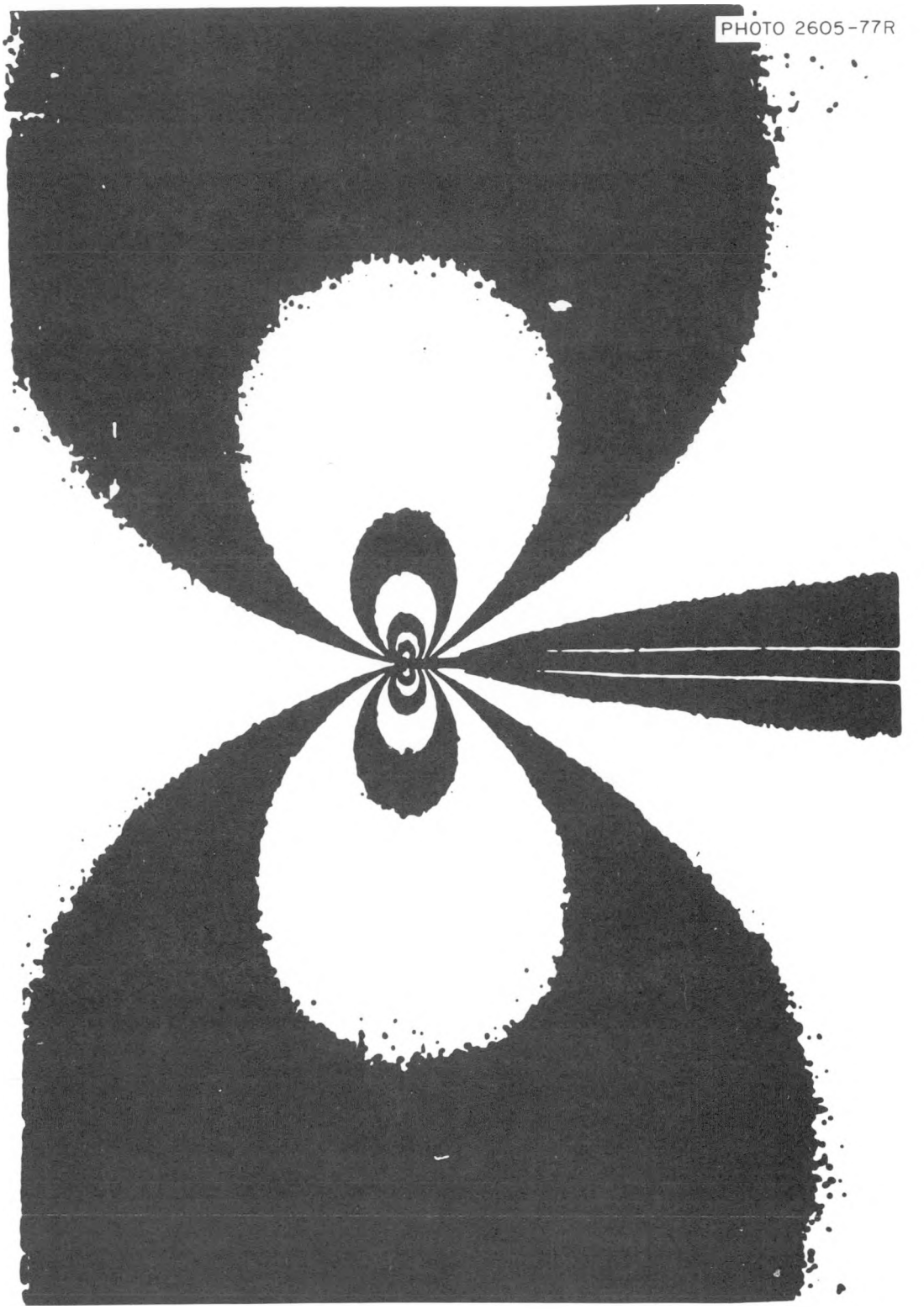

Fig. 2.3. Typical mode I fringe pattern.

where N is the stress fringe order, f is the material fringe value, and t' is the slice thickness parallel to the crack front; one can determine experimentally the zone in which Eq. (1) is valid by rewriting the equation in the normalized form:

$$\frac{\tau_{max}(8\pi r)^{1/2}}{p(\pi a)^{1/2}} = \frac{K_I}{p(\pi a)^{1/2}} + \frac{B(8\pi r)^{1/2}}{p(\pi a)^{1/2}} \tag{3}$$

or

$$\frac{K_{AP}}{p(\pi a)^{1/2}} = \frac{K_I}{p(\pi a)^{1/2}} + \frac{B(8)^{1/2}}{p}\left(\frac{r}{a}\right)^{1/2}, \tag{4}$$

where $K_{AP} = \tau_{max}(8\pi r)^{1/2}$ is defined as "apparent" SIF and p is the internal pressure. Equation (4), when plotted as $K_{AP}/p(\pi a)^{1/2}$ vs $(r/a)^{1/2}$, yields a straight line which when extrapolated to the origin will yield $K_I/p(\pi a)^{1/2}$, the normalized SIF.

The above approach for mode I loading has been extended to cover the mixed-mode[6,11] situation also.

In general, when mode I loads are applied to the crack tip, blunting at the crack tip occurs and produces a nonlinear zone that extends roughly out to a distance r/a = 0.04 from the crack tip along $\theta = \pi/2$. Moreover, the linear zone described by Eq. (4) tends to extend substantially from the crack tip in problems with slowly varying effects along the flaw border (as in the two-dimensional case). Conversely, a constriction at the singular zone occurs in problems with strong three-dimensional effects. However, if a linear zone is present in the raw data plot of normalized apparent SIF vs $(r/a)^{1/2}$, the presence of the desired data zone is assured.

2.1.3 Experiments

The model geometry used in phase I is shown in Fig. 2.4. The BWR model geometry for phases II and III is given in Fig. 2.5, and as assembled model is shown in Fig. 2.6. Two nozzles are located at diametrically opposite positions for both phases II and III. The test procedure is given below.

ORNL–DWG 78–5986

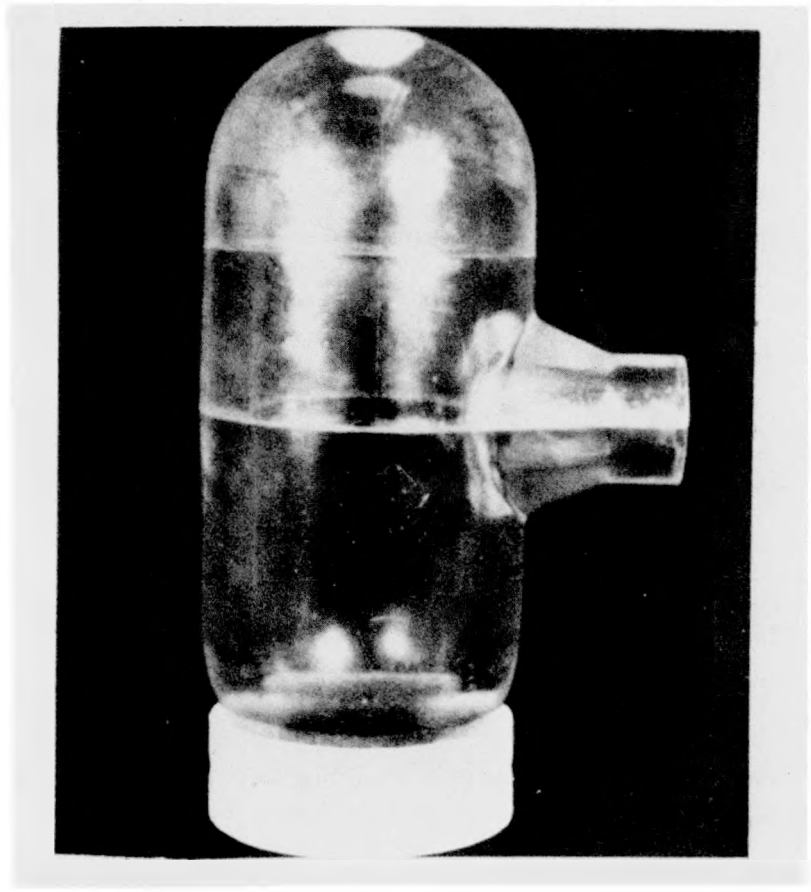

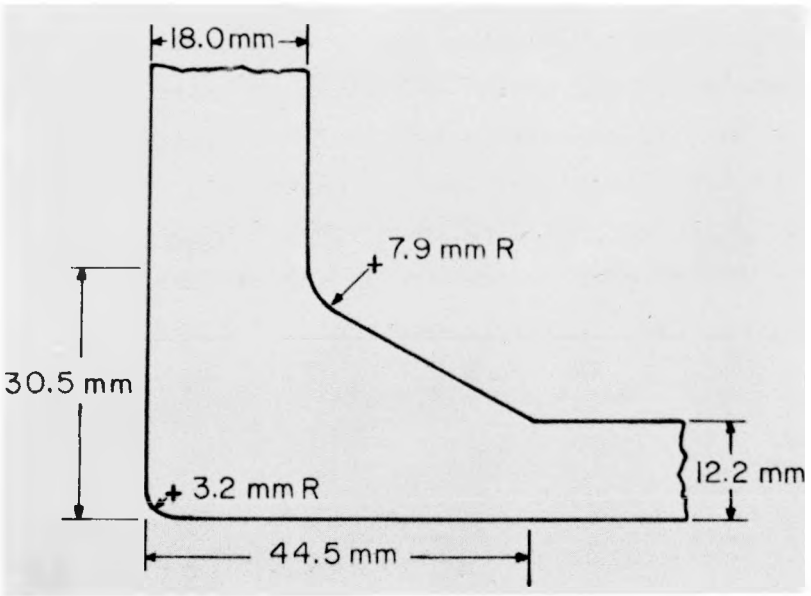

Fig. 2.4. Phase I geometry (ITV). Vessel inside radius = 43.2 mm, wall thickness = 18.0 mm; nozzle nominal radius (r_z) = 13.6 mm, wall thickness = 12.2 mm.

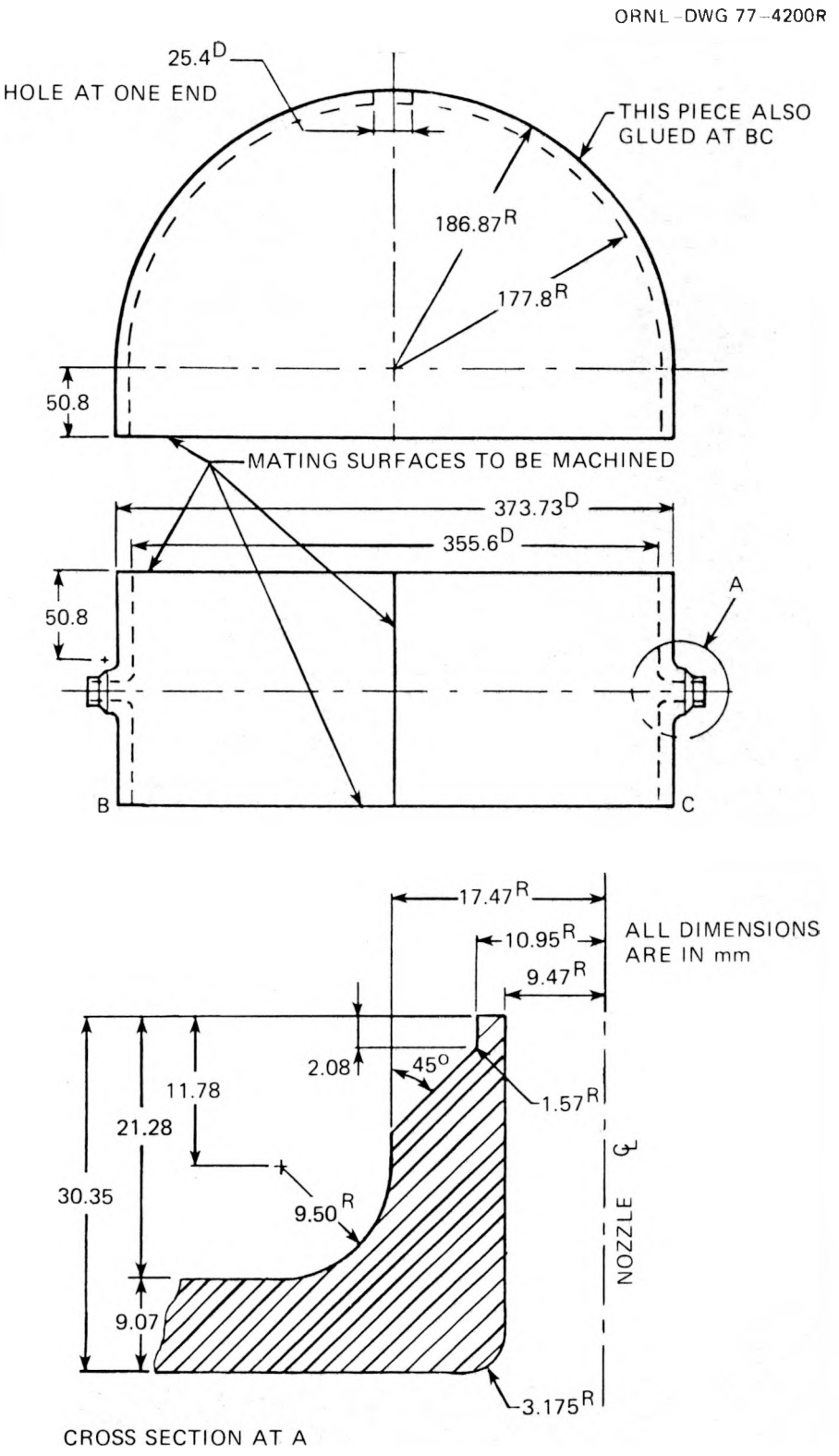

Fig. 2.5. Phase II and III BWR geometry.

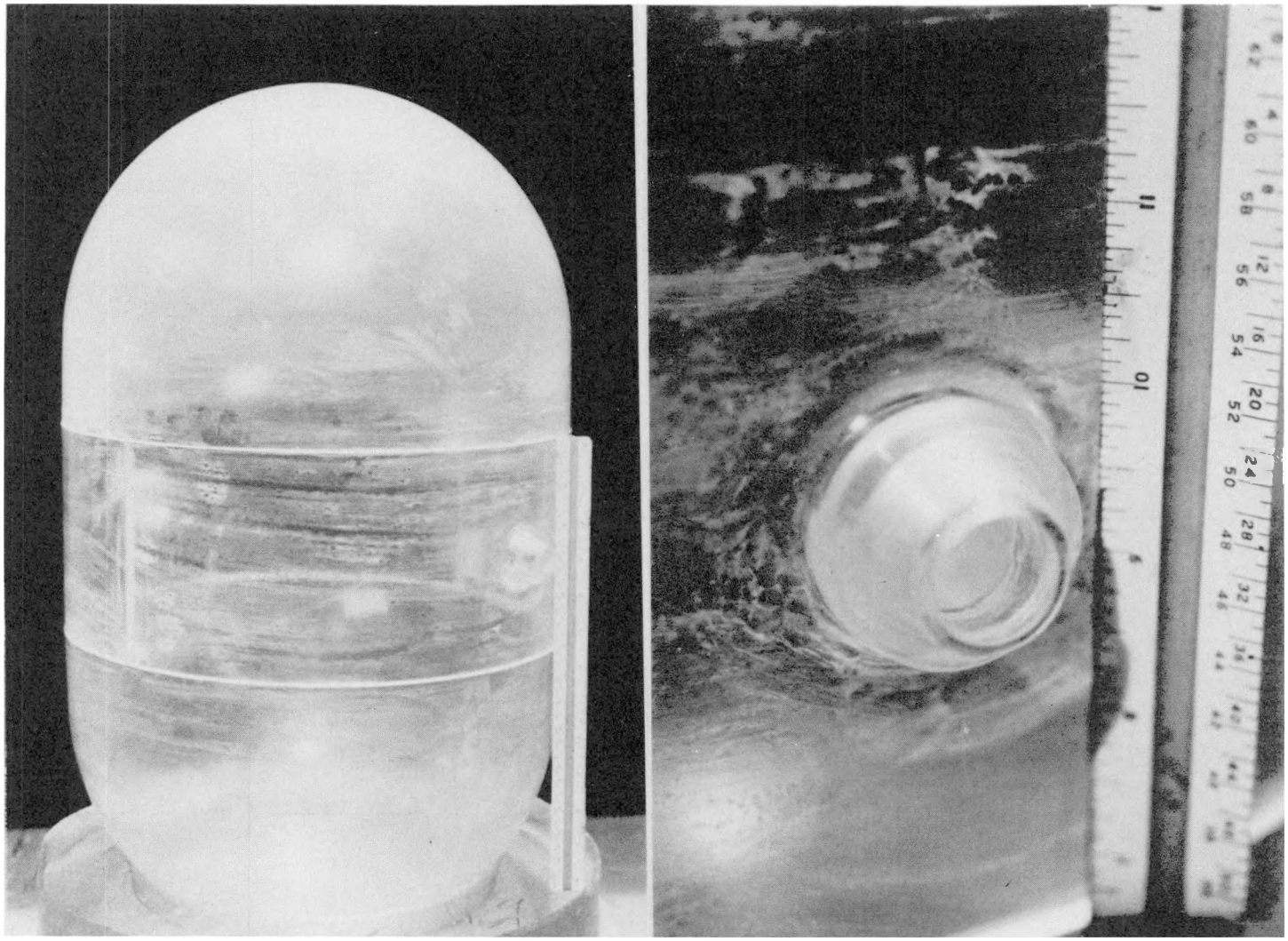

Fig. 2.6. Assembled model BWR and closeup of nozzle.

1. Starter cracks were introduced into the "inner" surface of the juncture of the vessel wall with the nozzle at point P (Fig. 2.2) and the photoelastic models were glued together, placed on a soft base in a stress freezing electric oven, and heated to a critical temperature.

2. Vessels were then pressurized while being supported in soft, surface-matching, part-spherical bases. These loads were increased until the flaws were grown to desired dimensions, after which the models were cooled under reduced load to room temperature, freezing in both fringe and deformation fields.

3. Slices were then removed mutually orthogonal to the flaw border and the flaw surface at intervals along the flaw border. These slices were coated with a matching index fluid and analyzed via the Tardy Method in a crossed circular polariscope at about 10× utilizing a white light field and reading tint of passage.

4. Optical data were introduced into a least-squares computer program which extracted estimates of the SIF.

Use of a typical set of data to estimate the SIF for a slice is shown in Fig. 2.7.

2.1.4 Summary of data and results to date

SIF values from phase I for the ITV models are summarized in Fig. 2.8. The upper part of the figure shows that, to within an experimental scatter of about 7%, the stress intensities near the central region of the flaw tend to increase with increasing flaw size. The SIF varies more along the deeper flaws than the shallow ones. The lower part of the figure also focuses on the central part of the flaw border. However, the flaw grows more rapidly near the walls than in the center, producing a flattening* of the flaw border in the central region as seen in Fig. 2.9. In one test, the flaw was driven completely through the model, producing a leak at the juncture of the vessel wall with the nozzle fillet (point Q, Fig. 2.9) and extended to RS.

---

*This effect has been observed in fatigue cracks in A-508 reactor vessel steel models.[16]

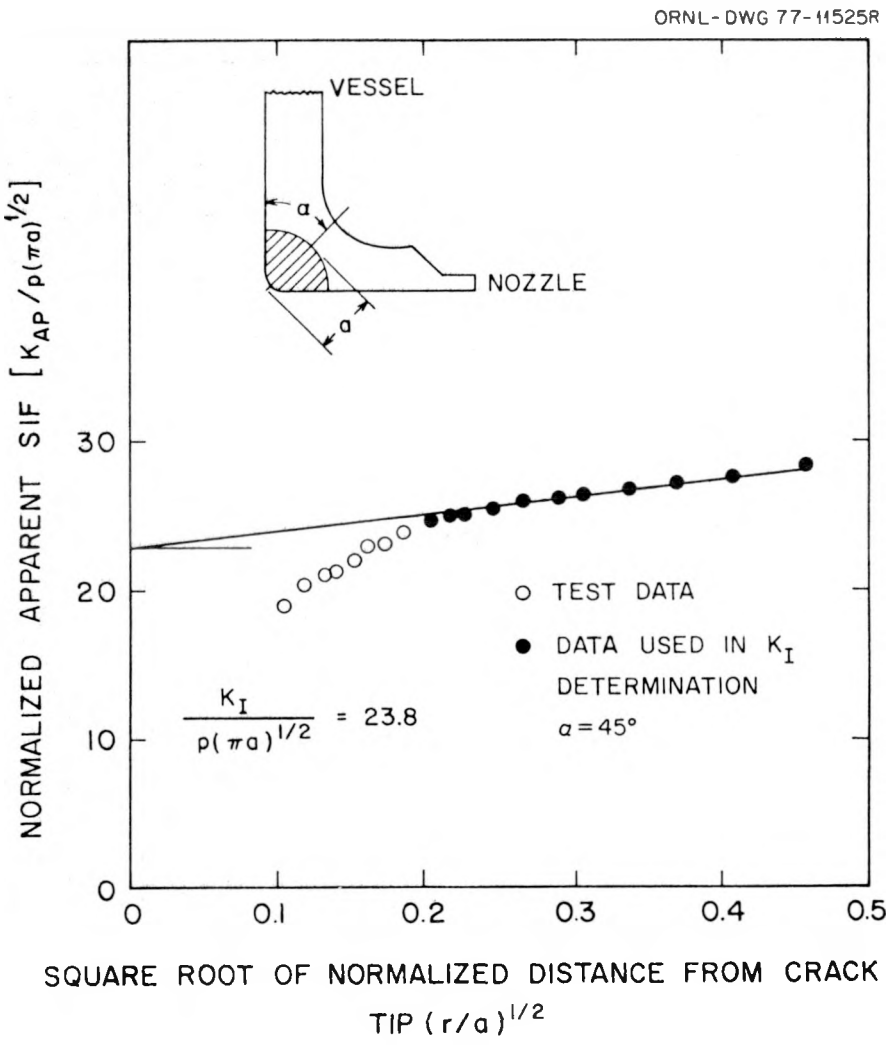

Fig. 2.7. SIF estimate from test data — typical curve.

Table 2.1 provides loads and flaw geometries studied in phase II; SIF values from phase II for the BWR models shown in Fig. 2.10 reveal the same trends found in phase I. However, it was possible to obtain data on flaws 0 and IAV which had not grown out of the fillet area, and these results showed an SIF distribution opposite that observed in the ITV and deeper BWR flaws. For the smallest flaw (0), only one central slice was obtained; this was taken from the middle third of the flaw and is shown as the single and lowest data point in the upper part of Fig. 2.10. The flattening of the flaw borders seen in the ITV flaws was also present in

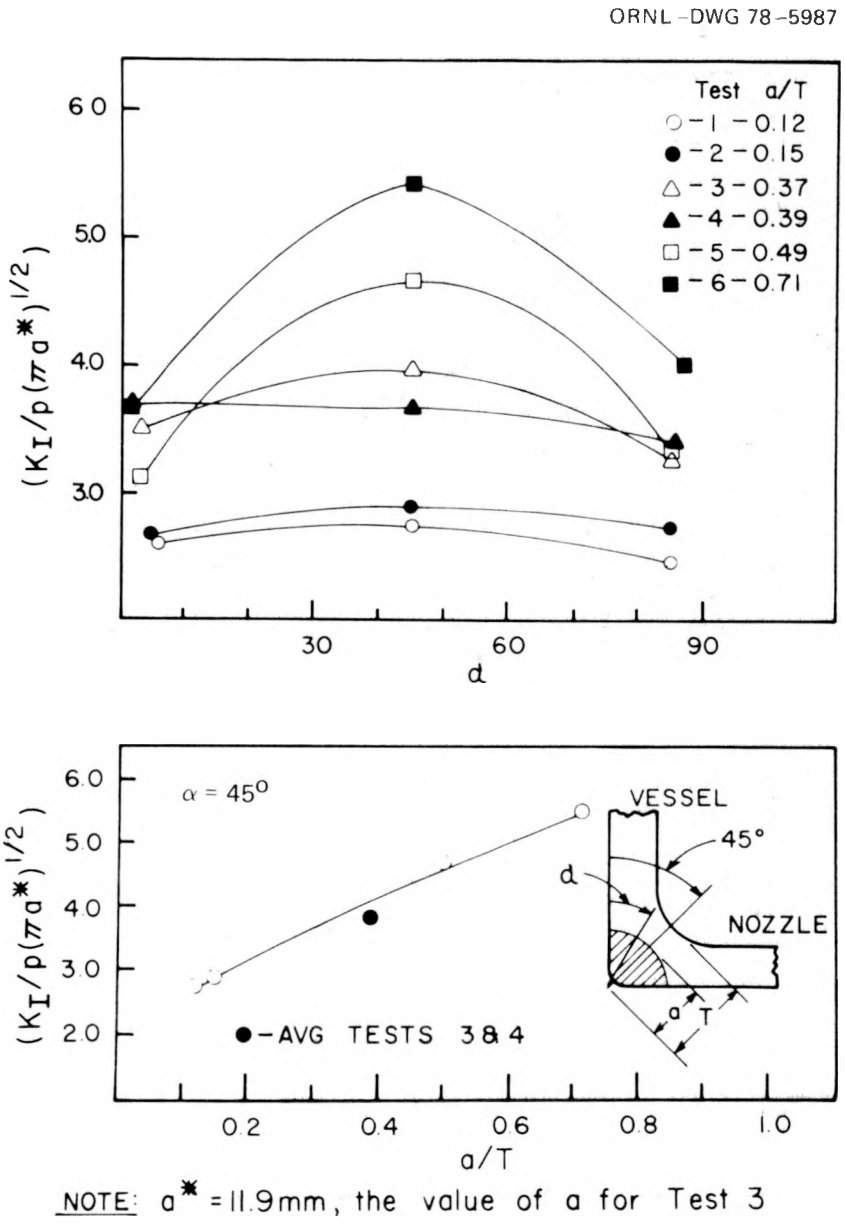

Fig. 2.8. SIF distributions of ITV models.

the BWR flaws (Fig. 2.11) and is highlighted by comparison with quarter-elliptic curves.

In addition to the results noted above, one test (two nozzles) in phase III has been conducted on the same model geometry studied in phase II (Fig. 2.5) but with the flaws located in the plane 90° from the longitudinal plane (flaw orientation C in Fig. 2.1). One of these flaws was

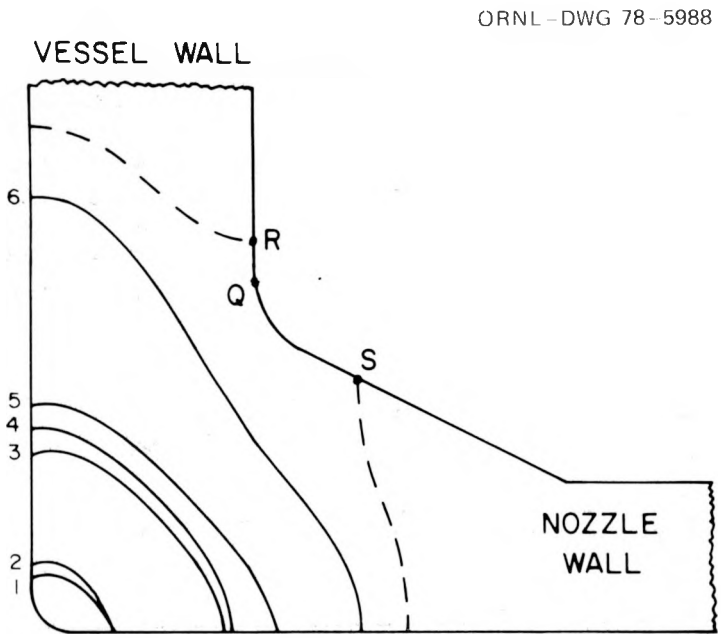

TEST	1	2	3	4	5	6
a_V (mm)	5.1	5.6	14.0	16.0	18.3	36.3
a_N (mm)	5.6	5.6	14.0	15.0	18.5	26.6
a (mm)	3.9	4.8	11.9	12.4	15.5	22.4
a/T	0.12	0.15	0.37	0.39	0.49	0.71

T = 31.8 mm FOR ALL TESTS

Fig. 2.9. Crack shapes in ITV models.

Table 2.1. Loads and flaw geometry for phase II tests of BWR models

Test parameter[a]	Test No.							
	0	IAV[b]	IIA	IIB	IIIA	IVB	VA	VI
p, kPa	4.72	3.20 ± 0.16	2.76	2.76	2.62	3.11	3.36	4.72
a_v, mm	1.78	2.62 ± 0.13	10.67	10.16	16.51	5.09	8.13	6.35
a_n, mm	3.30	4.06 ± 0	10.67	10.16	13.72	6.37	8.89	7.11
a, mm	1.30	2.08 ± 0	8.56	7.96	12.19	4.32	6.74	5.02
a/T	0.087	0.14 ± 0	0.57	0.53	0.81	0.29	0.44	0.33

[a] T = 15.1 mm for all tests.

[b] Average of three tests.

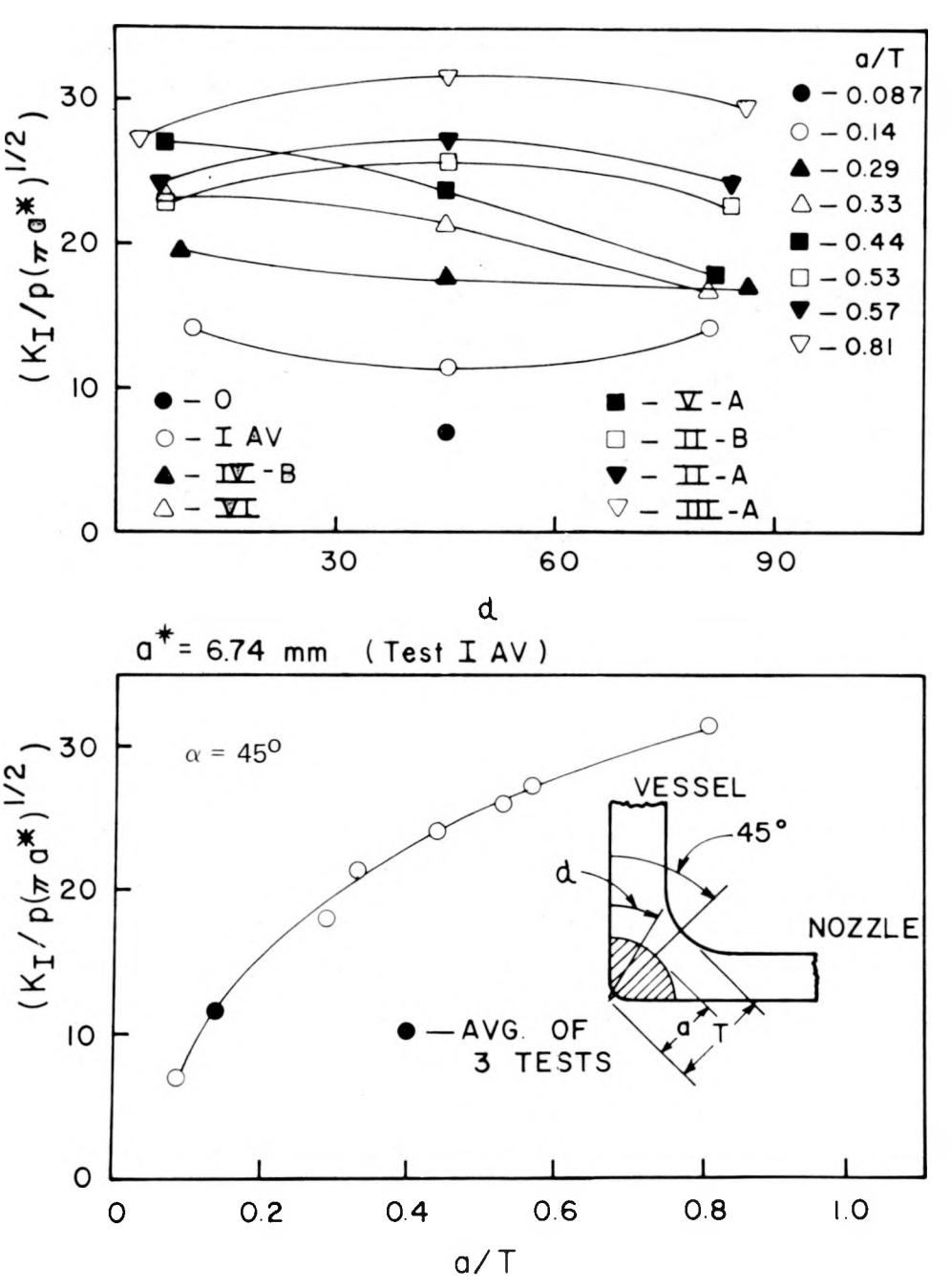

Fig. 2.10. SIF distributions of BWR models.

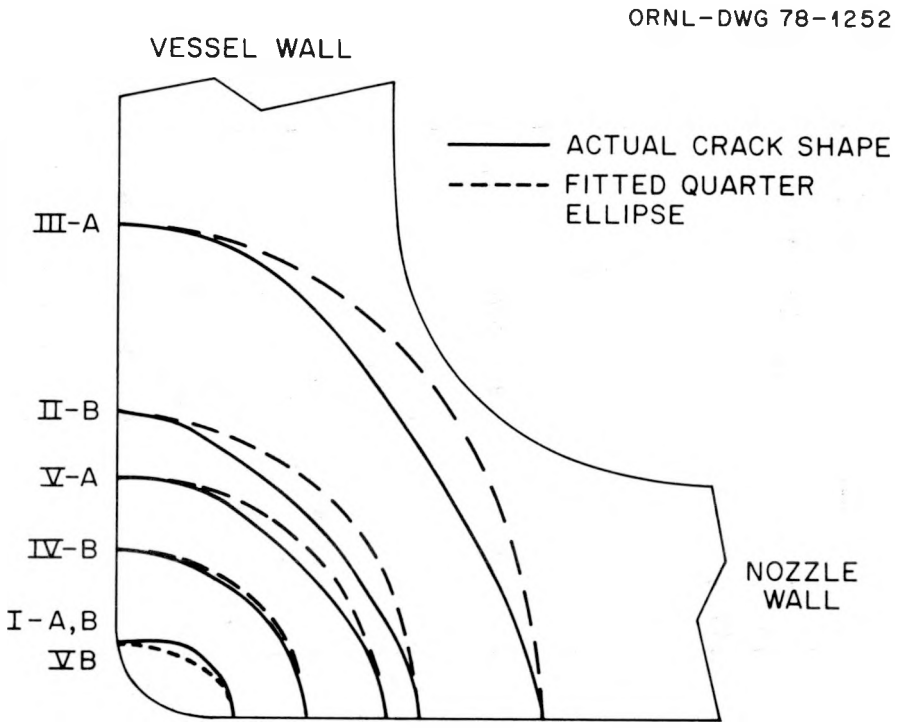

Fig. 2.11. Crack shapes in BWR models.

fairly shallow (a/T $\approx$ 0.15) and one was moderately deep (a/T $\approx$ 0.55). These flaws required about twice as much pressure to grow them as that required for the flaws grown from orientation A (Fig. 2.1), indicating a strong influence of the nominal vessel wall stress. Moreover, the flaws remained in their starter planes (Fig. 2.1) throughout growth. This is to be expected, since a slowly growing flaw should tend to orient itself normal to a principal stress, and the plane of the starter crack for orientation C is normal to a principal stress because it is a plane of symmetry. Data from these tests are currently being analyzed.

2.1.5 Discussion of results

This section is composed of three parts: (1) a comparison of the results of phases I and II with other studies; (2) an assessment of the ITV as a conservative prediction of local nozzle crack conditions in thin-walled BWR geometries; and (3) the use of the results of this study to improve rational design procedures.

However, before discussing these parts, some general observations appear to be in order. First, the entire effort of the present study (phases I, II, III) is directed toward local field stress analysis of *stably* grown flaws (as in fatigue) and, as such, is not generally related to fracture toughness considerations associated with *unstable* flaw growth. That is, the threshold value of the SIF at a point along the flaw border required to produce flaw growth there is not necessarily the plane strain fracture toughness of the material.

It is clear from Figs. 2.8 through 2.11 that, when flattening of the flaw borders occurs in the central region of the flaw, flaw growth rates are smaller there than at the surface even though the opposite is true for the SIFs. This may be explained qualitatively through the simplified crack growth rate equation:

$$\frac{da}{dN} = C(\Delta K)^n \quad . \tag{5}$$

It suggests that the material coefficients C and n, as determined from flaw growth tests on two-dimensional specimens of known ΔK, must be varying in the three-dimensional problem; that is, all the geometric effects are not captured in ΔK. Alternatively, if one assumes that

$$\frac{da}{dN} \propto \text{COD (crack opening displacement)} \ ,$$

it can be shown that[17]

$$\frac{da}{dN} = A' \left(\frac{\Delta K}{E}\right)^2 \quad . \tag{6}$$

The authors conjecture that, in the central region of the nozzle corner flaw, a state of triaxial tension is built up. This creates a stiffening effect or an increase in the apparent elastic modulus, resulting in a reduced crack growth rate as indicated by Eq. (6). They also feel that this stiffening effect decreases as one approaches the points of intersection of the flaw border with the boundaries. With these ideas in mind, we turn to the main elements of our discussion.

Comparison of results of phases I and II with other studies. The authors are aware of only one other study involving a nozzle corner crack in a thick-walled vessel of the same geometry that they investigated. This study was conducted by Derby[13] at ORNL and consisted of epoxy models with machined slots from which fatigue cracks were grown to various sizes and SIFs obtained from residual static strength tests. The comparison with these results shown in Fig. 2.12 indicates agreement to within experimental scatter except for very shallow flaws ($a/T \leq 0.2$). For these cracks, Derby's test scatter was about half the difference in the two sets of results, and, since he used a machined starter notch, his fatigue cracks may have been different than those studied in phase I.

A number of analytical studies have been conducted of SIF distributions along nozzle cracks in thin-walled pressure vessels (phase II). These studies have indicated SIF distributions that are concave upward,[2,3] nearly constant,[1] and concave downward,[4] depending upon crack shapes and sizes. Phase II results indicate that all three types of distributions are possible in the same nozzle juncture geometry, depending again upon crack size and shape.

One of the most popular analyses of this problem in current reactor technology is due to Gilman and Rashid (G-R)[18] and involves a geometry quite similar to that studied in phase II. Figure 2.13, a comparison of the average of the experimental SIF values obtained from phase II with the G-R analysis, indicates agreement to within experimental scatter except for shallow flaws. The authors suggest that part of the discrepancy is due to the fact that the arbitrarily assumed quarter-circular shapes used in the G-R analysis do not create realistic geometries when they are within the corner fillet radius because they do not intersect the fillet boundary at right angles as do the authors' cracks; and so the crack shapes are quite different from those of the authors.

Collectively, these comparisons suggest that the work of phases I and II characterizes the moderate and deep flaw geometries for flaws at right angles to the vessel hoop stress to within reasonable engineering accuracy. Moreover, they conjecture that for very shallow flaws, normalized SIF values may be lower than previously predicted.

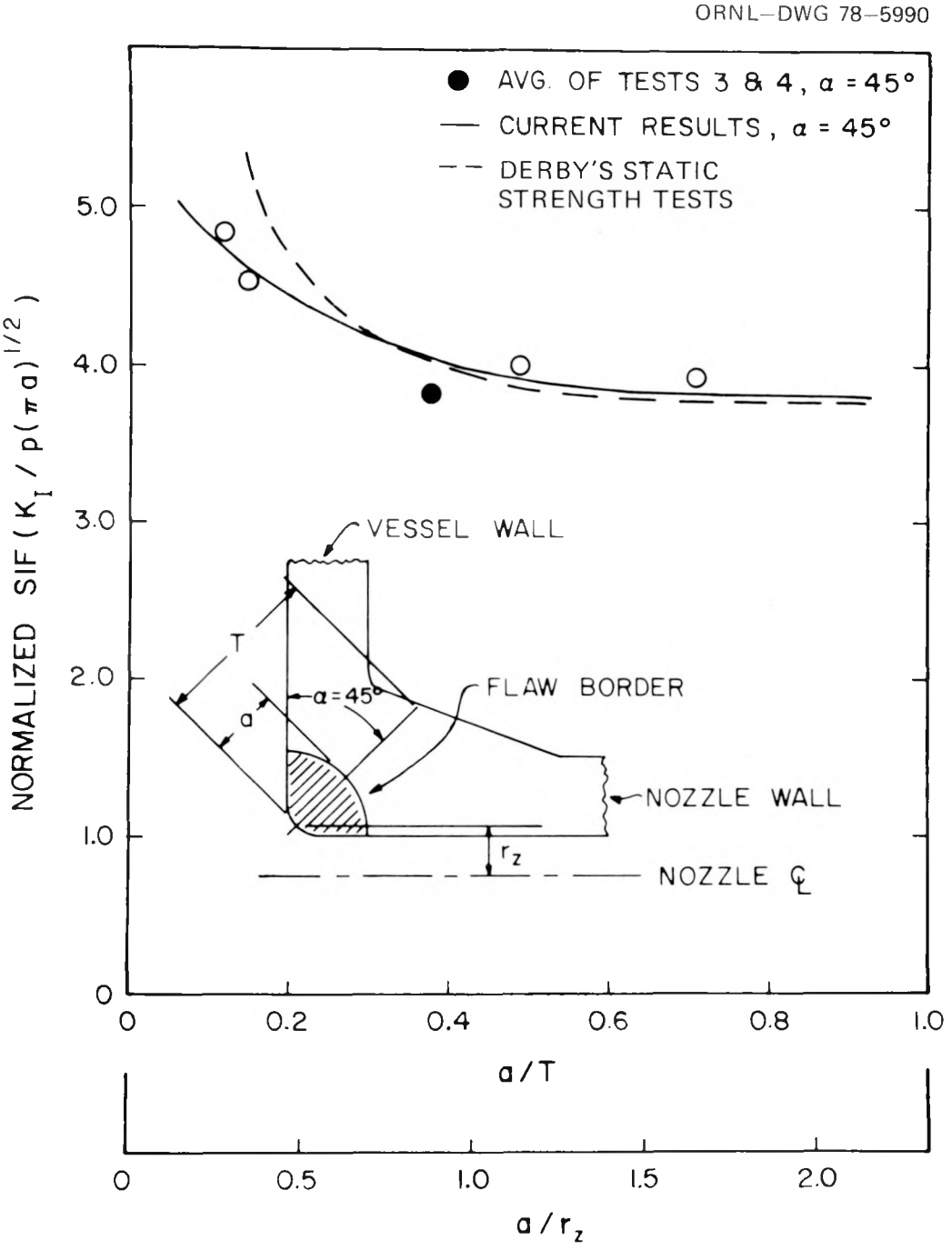

Fig. 2.12. Comparison of results of photoelastic and static strength tests (Ref. 13) of ITV models.

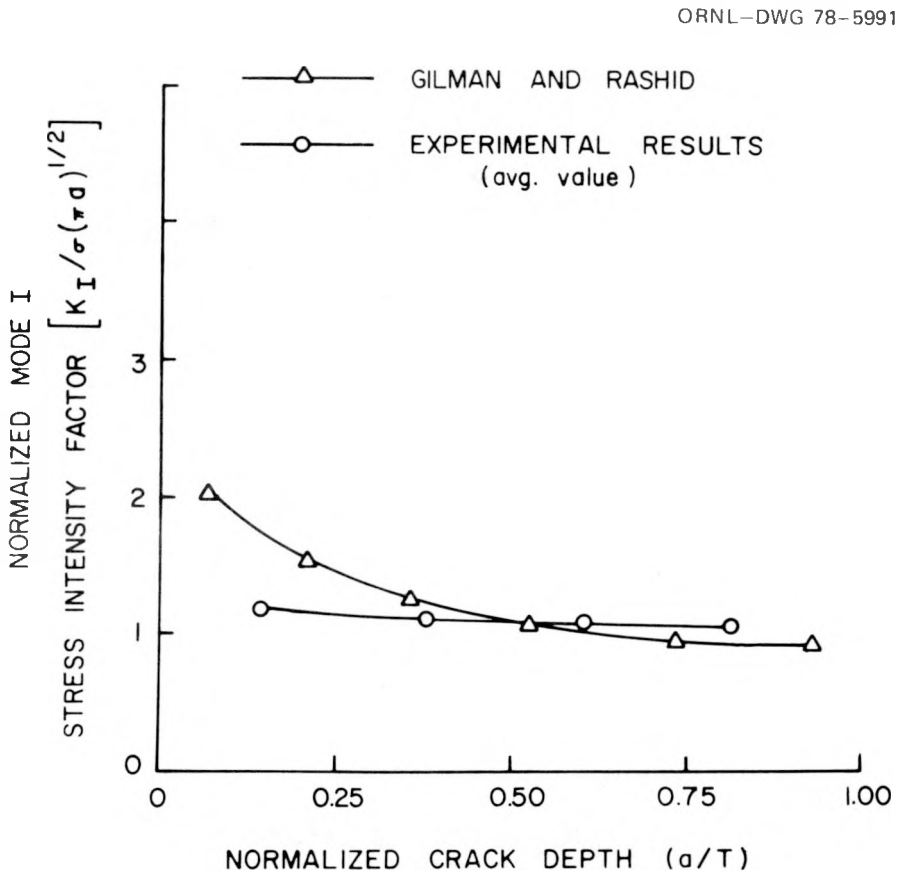

Fig. 2.13. Comparison of results of photoelastic tests of BWR models with analysis of Gilman and Rashid (Ref. 18).

An assessment of the ITV as a conservative prediction of local nozzle crack conditions in thin-walled vessel (BWR) geometries. An integral cost-effective feature of the HSST program has been the development and use of intermediate test vessels (ITVs) that are intended to conservatively simulate local cracked nozzle behavior in full-scale thin-walled vessels such as the BWR. Figure 2.14 represents an attempt to quantitatively summarize results gathered in phases I and II of the current study which appear to bear upon this subject. In normalizing SIF values for the ITV, $\bar{\sigma}$ represents the through-the-wall thickness average of the Lamé hoop stress.

In Fig. 2.14*a*, it should be noted that even though a/T values are the same for the two flaws, the flaw in the ITV is much deeper relative to the inner fillet radius than the BWR flaw, which has not grown out of

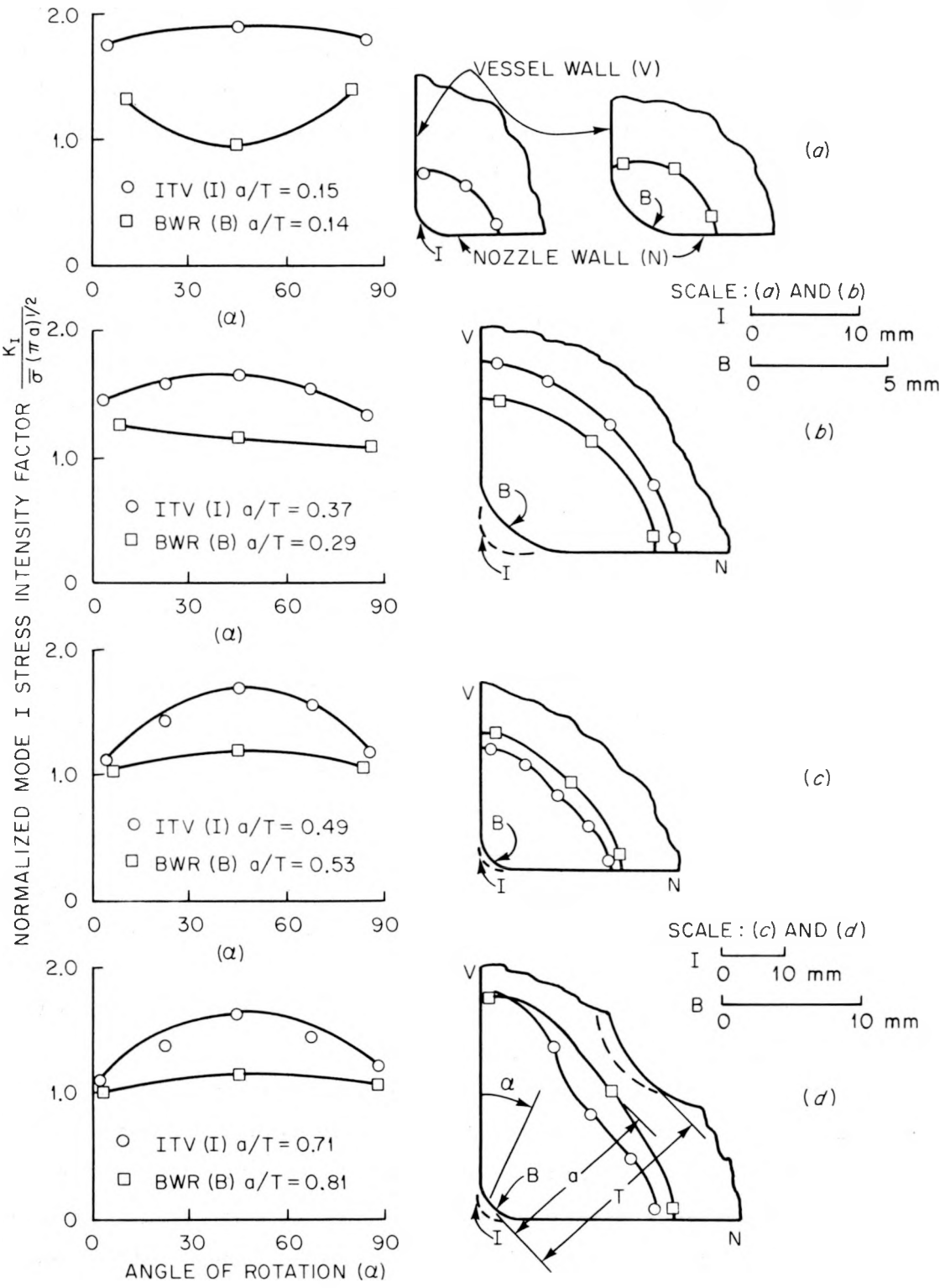

Fig. 2.14. Comparison of results of ITV and BWR model tests.

the fillet. This is because the ITVs were intentionally designed to have a conservatively high stress concentration at the fillet. Consequently, the difference in SIF curves here is not unexpected and this difference becomes smaller as the flaw grows deeper. In the opinion of the authors, Fig. 2.14 indicates that the ITV geometry locally reproduces crack shapes and stress fields present in the BWR with a margin of safety (in SIF values) of 20 to 50%.

Use of results of this study to improve rational design methods. In the organization of stress analysis information into a foundation upon which to build rational design procedures for dealing with three-dimensional cracked-body problems one must rely heavily upon capitalizing upon the capabilities of modern digital computing systems through numerical analyses. The flexibility of these analyses is materially enhanced by a myriad of discretization and hybrid techniques. Due to problem complexity, the applied mathematician may be forced to relax certain constraints in the interest of cost effectiveness. For the problem at hand, one such simplification has been the use of arbitrarily assumed simple curve shapes such as quarter-circles or quarter-ellipses. This may significantly alter the local stress field and hence the values and distributions of SIFs. This may result in a solution which, while quite accurate for the assumed geometry, may differ substantially from SIF distributions around a "natural" flaw of different geometry. In the authors experience, natural flaws characteristically exhibit lower SIF gradients along natural rather than along arbitrary flaw borders. The authors suggest that the use of real or natural flaw shapes in computer codes will improve analytical-experimental correlation.

The frozen stress technique is not without its own constraints. Its use is restricted to essentially incompressible linearly elastic materials where only small-scale yielding is involved. However, the combined influence of these constraints in studying stable flaw situations is believed not to exceed the range of the experimental scatter which normally lies between 5 and 10%.

Additional studies extending the frozen stress method to cracks with orientations B and C (Fig. 2.1) in phase III are in progress.

References

1. T. K. Hellen and A. H. Dowling, "Three Dimensional Crack Analysis Applied to an LWR Nozzle-Cylinder Intersection," *Int. J. Pressure Vessels Piping* 3, 57–74 (1975).

2. J. Reynen, "On the Use of Finite Elements in the Fracture Analysis of Pressure Vessel Components," ASME Paper 75-PVP-20, June 1975.

3. M. G. J. Broekhoven and H. A. C. M. Spaas, *Application of the Finite Element Technique to a Complex 3-D Elastic Problem (Nozzle Junction with Cracks)*, Rep. MMPP101, Laboratory for Nuclear Engineering Delft University of Technology (August 1974).

4. W. Schmitt et al., "Calculation of Stress Intensity Factors for Cracks in Nozzles," *Int. J. Fract.* 12(3), 381–90 (June 1976).

5. D. G. Smith and C. W. Smith, "A Photoelastic Investigation of Closure and Other Effects upon Local Bending Stresses in Cracked Plates," *Int. J. Fract. Mech.* 6(3), 305–18 (September 1970).

6. D. G. Smith and C. W. Smith, "Photoelastic Determination of Mixed Mode Stress Intensity Factors," *Eng. Fract. Mech.* 4(3), 357–66 (1972).

7. C. W. Smith, J. J. McGowan, and M. Jolles, "Effects of Artificial Cracks and Poisson's Ratio upon Photoelastic Stress Intensity Determination," *Exp. Mech.* 16(5), 188–93 (May 1976).

8. J. J. McGowan and C. W. Smith, "Stress Intensity Factors for Deep Cracks Emanating from the Corner Formed by a Hole Intersecting a Plate Surface," *Mechanics of Crack Growth*, ASTM STP 590, American Society for Testing and Materials, pp. 460–76, 1976.

9. M. Jolles, J. J. McGowan, and C. W. Smith, "Use of a Hybrid Computer Assisted Photoelastic Technique for Stress Intensity Determination in Three-Dimensional Problems," Computational Fracture Mechanics, ASME-AMD-SP *Proceedings of Second National Congress on Pressure Vessels and Piping*, E. F. Rybicki and S. E. Benzley, eds., pp. 63–82, 1975.

10. C. W. Smith, M. Jolles, and W. H. Peters, "Stress Intensity Determination in Three-Dimensional Problems by the Photoelastic Method," *Proceedings of the Second International Conference on Mechanical Behavior of Materials*, pp. 235–39, 1976.

11. C. W. Smith, M. Jolles, and W. H. Peters, "Stress Intensities for Cracks Emanating from Pin Loaded Holes," *Flaw Growth and Fracture, Proceedings of 10th National Symposium on Fracture Mechanics*, ASTM STP 631, pp. 190–201, October 1977.

12. C. W. Smith, M. Jolles, and W. H. Peters, "Stress Intensities in Flawed Pressure Vessels," *Proceedings of the Third International Conference on Pressure Vessel Technology*, Part II, Materials and Fabrication, pp. 535–44, April 1977.

13. R. W. Derby, "Shape Factors for Nozzle Corner Cracks," *Exp. Mech.* 12(12), 580–84 (December 1972).

14. C. W. Smith, M. Jolles, and W. H. Peters, "Stress Intensities for Nozzle Cracks in Reactor Vessels," *Exp. Mech.* 17(12), 449–54 (December 1977).

15. C. W. Smith, W. H. Peters, and M. I. Jolles, "Stress Intensity Factors for Reactor Vessel Nozzle Cracks" (Invited Paper), ASME Paper 77-PVP-30, *Journal of Pressure Vessel Technology* (in press).

16. C. W. Smith, M. Jolles, and W. H. Peters, "An Experimental Study of the Plate-Nozzle Tensile Test for Cracked Reactor Vessels," *Developments in Mechanics, Vol. 8, Proceedings of the 15th Midwest Mechanics Conference*, pp. 20–31, March 1977.

17. G. T. Hahn, M. Sarrate, and A. R. Rosenfeld, "Experiments on the Nature of the Fatigue Crack Plastic Zone," *Proceedings of the Air Force Conference on Fatigue and Fracture of Aircraft Structures and Materials*, AFFDL TR-70-194, pp. 425–50 (September 1970).

18. Y. R. Rashid and J. D. Gilman, "Three Dimensional Analysis of Reactor Pressure Vessel Nozzles," *Transactions of the First International Conference on Structural Mechanics in Reactor Technology*, Vol. 6, Paper 216, 21 pp., 1971.

04396

3. EFFECT OF HIGH-TEMPERATURE PRIMARY REACTOR WATER ON THE SUBCRITICAL CRACK GROWTH OF REACTOR VESSEL STEELS*,†

W. H. Bamford††
D. M. Moon†† L. J. Ceschini††

The objective of this continuing program is to characterize the fatigue-crack-growth rate properties of ferritic vessel steels exposed to PWR primary coolant environments. Three environmental chambers are being used, and the following areas are being investigated:

Ramp- and hold-time effects (2T WOL specimens)	1 chamber (14 MPa, 288°C) 1 chamber (0.14 MPa, 93°C)
Crack growth rate at high ΔK (4T CT, 4T WOL specimens)	1 chamber (14 MPa, 288°C)

3.1 Crack Growth in Weldments

Testing on this task was completed during the reporting period with the removal of specimen C-6, which is the sixth in a series of specimens from a submerged-arc weldment. The cracks in this series of specimens are oriented along the center of the weld, where the crack would be propagating along the direction in which a typical weld bead was laid. The weld and specimen geometry are described in detail in Ref. 1.

The crack growth rate results for specimen C-6 shown in Fig. 3.1 compare well with previous results on the same material (Fig. 3.2). This test was conducted with a sinusoidal loading of 1 cpm with an R ratio (K_{min}/K_{max}) equal to 0.74. As seen in Fig. 3.1, the crack growth was observed to increase with the range of applied stress-intensity factor for a time, after which a severe deceleration occurred. This retardation is not attributable to any testing anomalies but seems to be a characteristic of crack growth in welds. The retardation of the crack growth rate

---

*Work sponsored by HSST program under UCCND Subcontract 3290 between Union Carbide Corporation and Westinghouse Electric Corporation.

†Conversions from SI to English units for all SI quantities are listed on a foldout page at the end of this report.

††Westinghouse Electric Corporation.

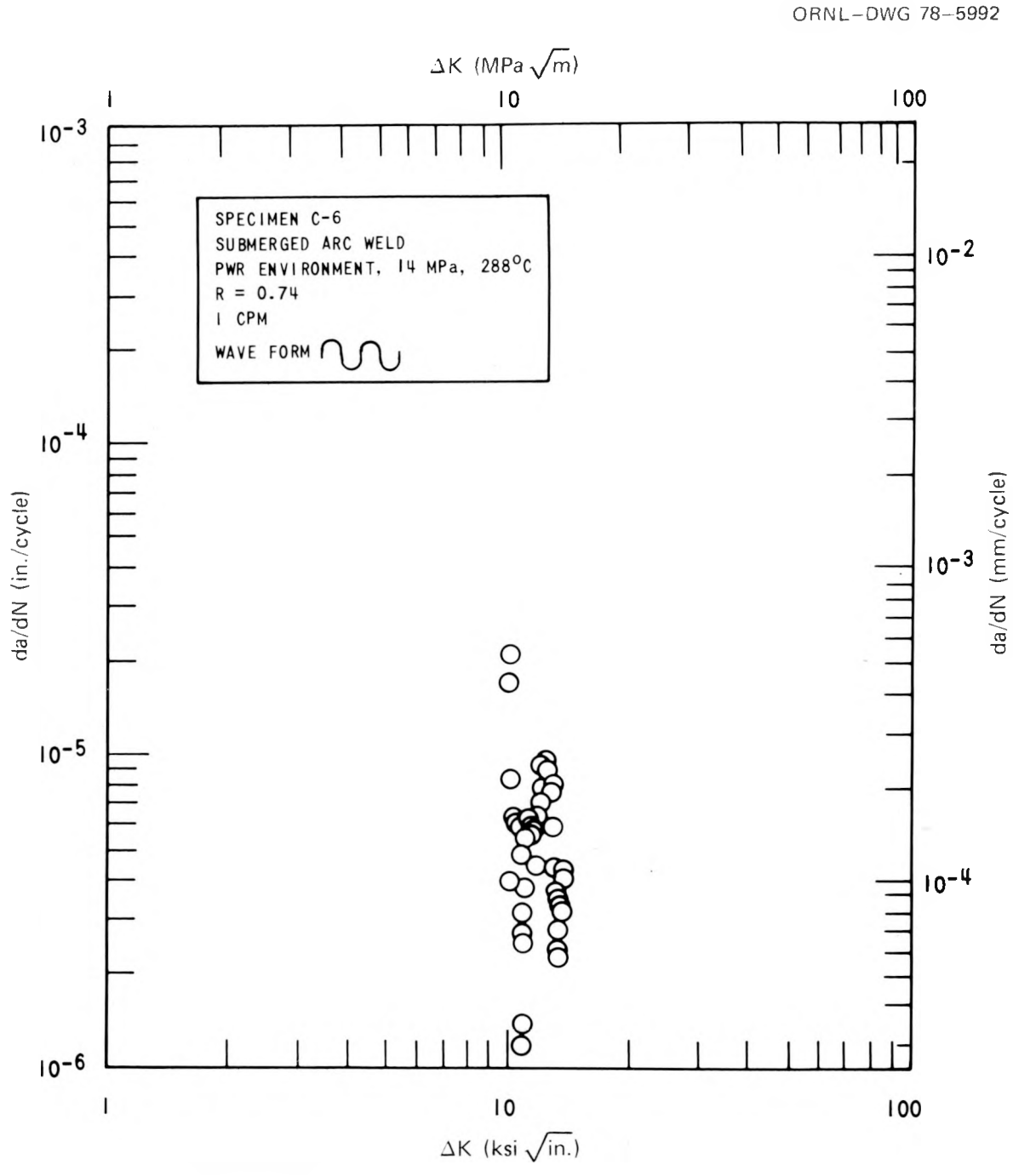

Fig. 3.1. Fatigue-crack-growth results for specimen C-6.

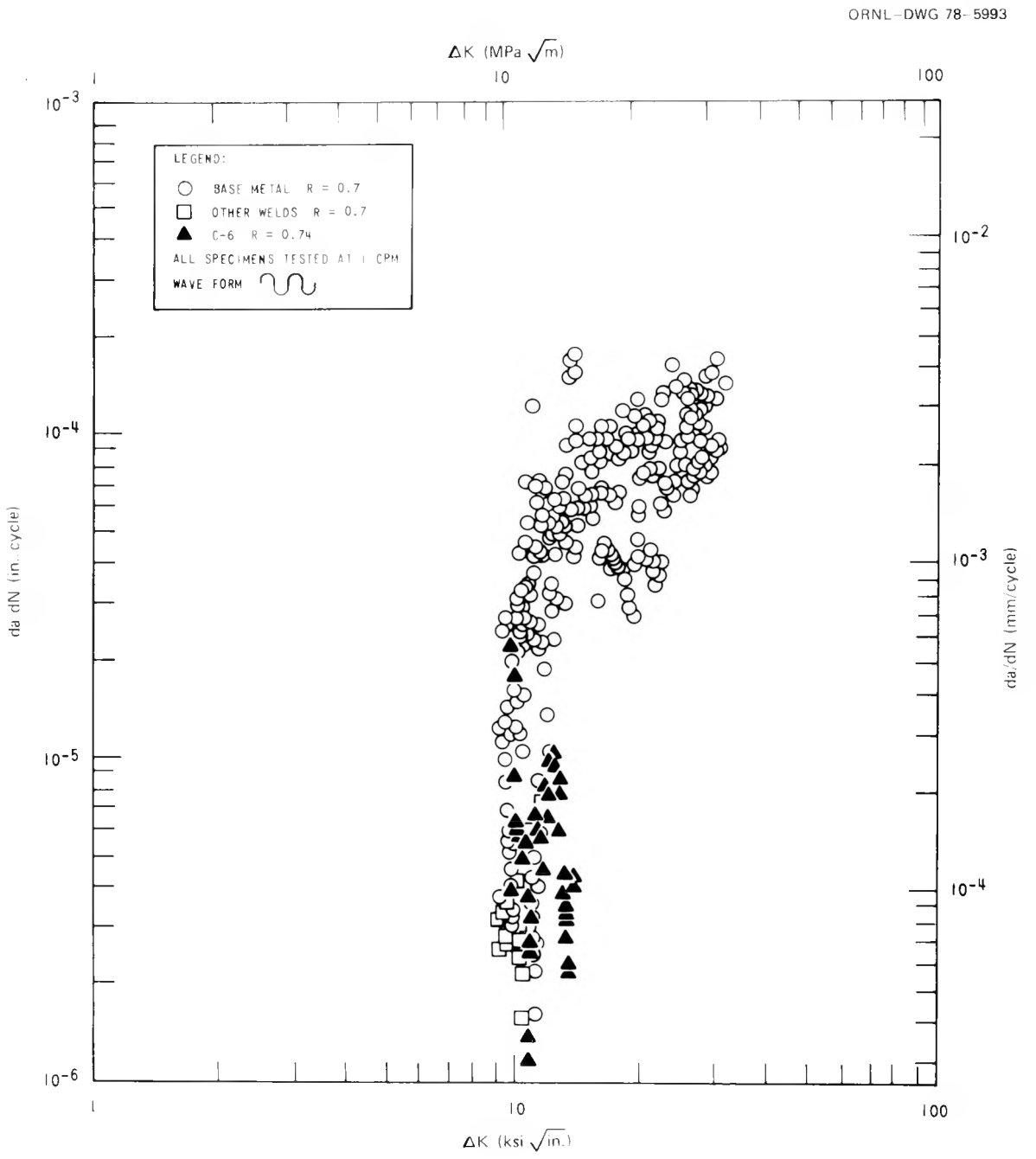

Fig. 3.2. Comparison of crack growth results for welds and base metal in PWR environment — high R ratio.

has been observed in earlier weld specimens in this series and seems to be particularly evident in tests conducted at high R ratios. This test was conducted for a period of about 6.5 months, resulting in a total growth of less than 20 mm, as compared with total growth of nearly 44.5 mm usually obtained from the 2T WOL specimen. The test was terminated after this time because growth had nearly stopped. Specimen C-6 was tested at the highest value of R ratio yet attempted in these weld specimens, and the results could have potentially important consequences from the standpoint of applications.

The growth of a crack in a weld of a pressure vessel is likely to be very slow for loadings imposed with high values of R ratio. Even crack growth in weldments subjected to low R ratio loadings will be slower than in the base metal, because reversals occur here as well.[1,2] Thus welds, which are an essential part of each vessel and are carefully inspected as a potential source of flaws, appear to be somewhat more resistant to crack propagation than the base metal.

3.2 Ramp- and Hold-Time Effects

The investigation of ramp- and hold-time effects has been under way for nearly two years and is being pursued with 50.8-mm-thick WOL-type specimens of A508 class 2 forging material. Tests are being coordinated with the Naval Research Laboratory, and identical material is being used by both laboratories. The test conditions are summarized in Table 3.1.

Results for specimen F-9, which was tested at an R ratio equal to 0.2 and is part of series "b" of the investigation, are shown in Fig. 3.3. The ramp and hold times were 1 min and the environment was simulated PWR water maintained at 14 MPa and 288°C.

Specimen F-9 shows crack growth behavior which has not been observed in previous tests in this series. The crack growth was significantly retarded after the first part of the test, when the applied stress-intensity factor range (ΔK) reached about 19.9 MPa $\sqrt{m}$. This change in growth rate was coincident with a shutdown of the test,* after which

*This shutdown was necessitated by a problem with the testing apparatus that resulted in a leak in the test chamber.

Table 3.1. Projected ramp- and hold-time tests of 2T WOL specimens in PWR environment, A508 class 2 forging material[a]

Test	Ramp time (min)	Hold time (min)
a1	Rapid, 1 sec	1
a2	Rapid, 1 sec	3
a3	Rapid, 1 sec	12
a4	Rapid, 1 sec	60
b1	1	1
b2	1	3
b3	1	12
b4	1	60
c1	5	1
c2	5	3
c3	5	12
c4	5	60
d1	30	1
d2	30	3
d3	30	12
d4	30	60

[a]Tests a4, b4, c3, c4, d2, d3, d4, which are very long time tests, will be done after the others are complete.

testing was continued at a lower applied ΔK, with a 1-min ramp and a 3-min hold time for about 3000 cycles. Very little growth occurred during this period, after which the original test conditions were reimposed on the specimen. The intermediate test conditions were imposed by a laboratory error in communication, and the only observable physical effect was a beachmark on the specimen.

Results of specimen F-9 are compared with earlier results of the ramp- and hold-time test series in Fig. 3.4. The crack growth behavior for the early part of the test compares very favorably with the earlier result obtained for specimen F-8 tested under the same conditions except for a lower temperature and pressure. After the interruption, however, the crack growth was significantly retarded, although it remained parallel to the previous data. This result unfortunately does not lead to a clear conclusion about the effects of ramp and hold time. As discussed

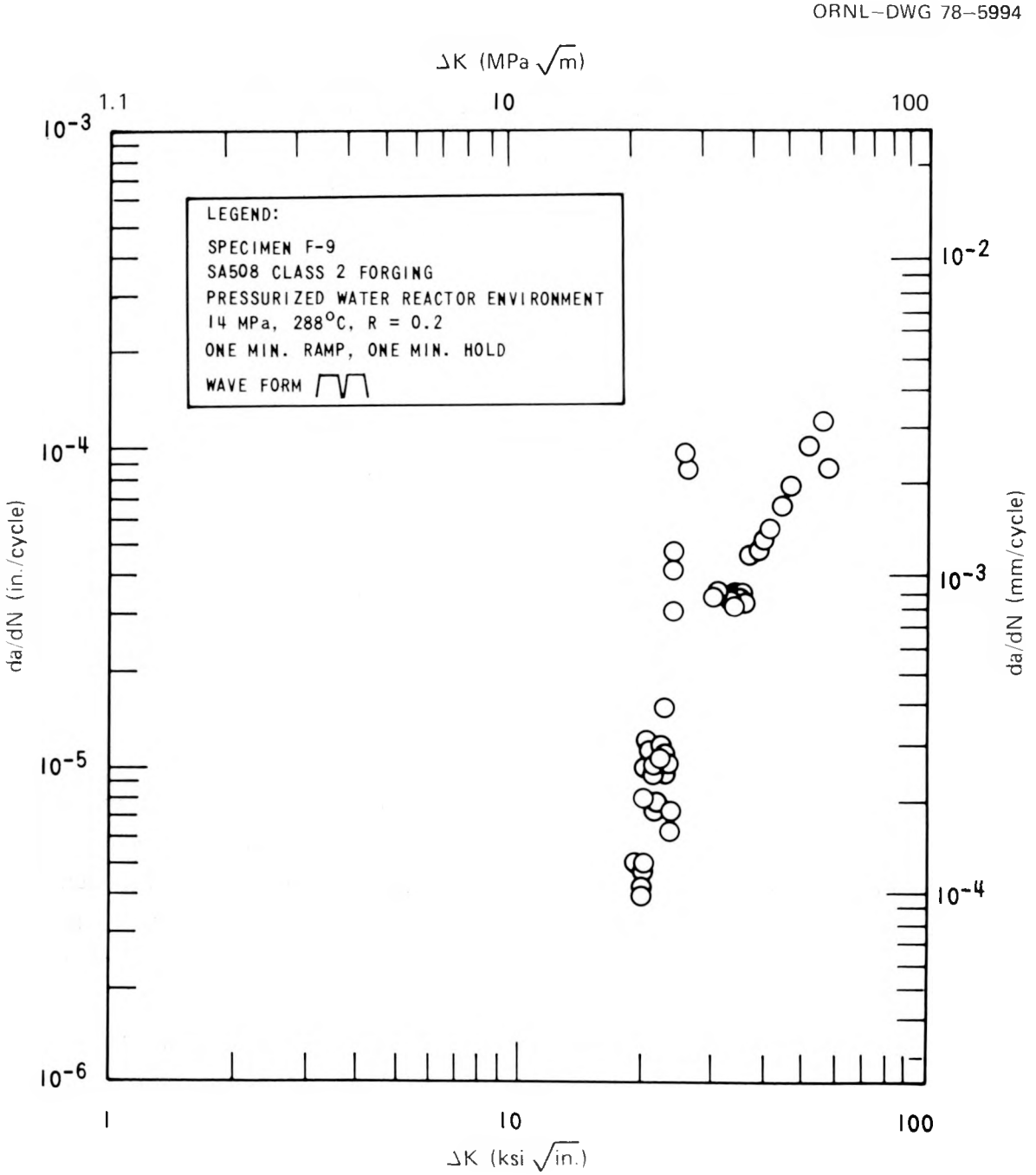

Fig. 3.3. Fatigue crack growth results for specimen F-9.

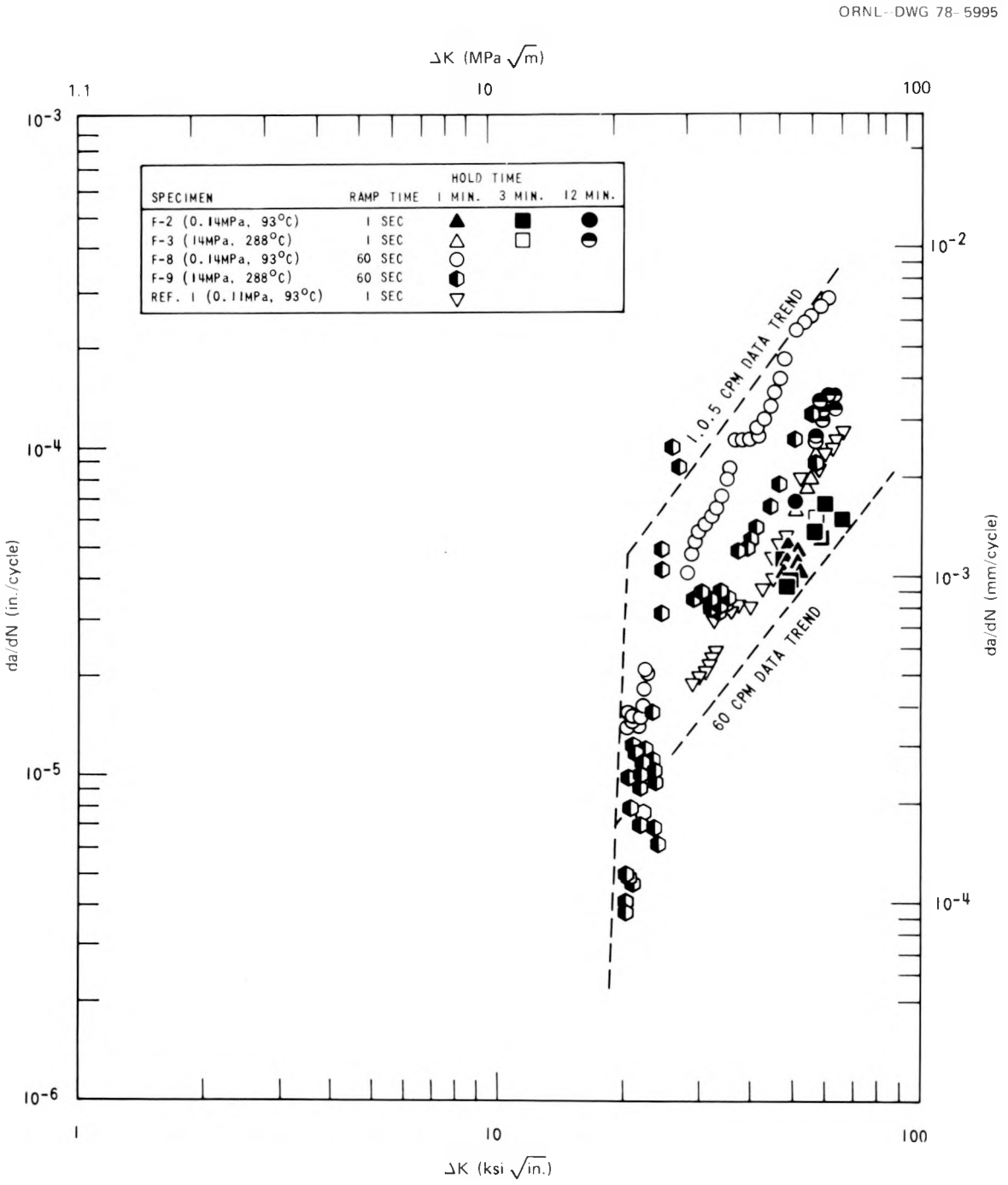

Fig. 3.4. Summary of ramp- and hold-time results for pressure vessel steels in PWR environment.

earlier,[1-3] the previous data have shown that hold time has no effect on the crack growth behavior and that ramp time is most important. A more definitive conclusion on this question may be reached when the results of two specimens now being tested are available, probably in the next reporting period. These are specimen F-10, being tested with a triangular wave and ramp time equal to 1 min, and specimen F-11, with a 1-min ramp and a 3-min hold time.

3.3 Crack Growth at High ΔK

Testing is continuing on specimen F-24 at 1 cpm and an R ratio of 0.2. This is a 101.6-mm-thick compact specimen which is being used to investigate crack growth behavior at higher values of ΔK than have previously been studied.

3.4 Mechanisms of Crack Growth

The mechanisms of fatigue crack growth in the present experiments are dependent on both the material and environment. Examination of the fracture surfaces indicates that different mechanisms of crack growth are occurring in the base metal and the weld specimens, as shown in Fig. 3.5.

In the base metal, both A533B and A508 class 2, all the crack propagation in the PWR environment occurs by ductile striation formation. The striation spacings measured agree completely with the macroscopic growth throughout the range of applied stress-intensity factor where measurements could be made. This agreement held for all values of R ratio and cyclic frequency, confirming the absence of any other environmentally induced cracking mechanism.

Another mechanism of crack growth, void coalescence, occurs in the weld specimens. This mechanism occurs in both air and PWR water environments, but the crack growth in the PWR environment is considerably enhanced, as has been previously observed. Crack propagation by void coalescence in ferritic steel has been observed previously in both base metal[4,5] and weld.[6] In the present experiments the transition in fractography from striations to void coalescence is related to the much

ORNL PHOTO 1176–78

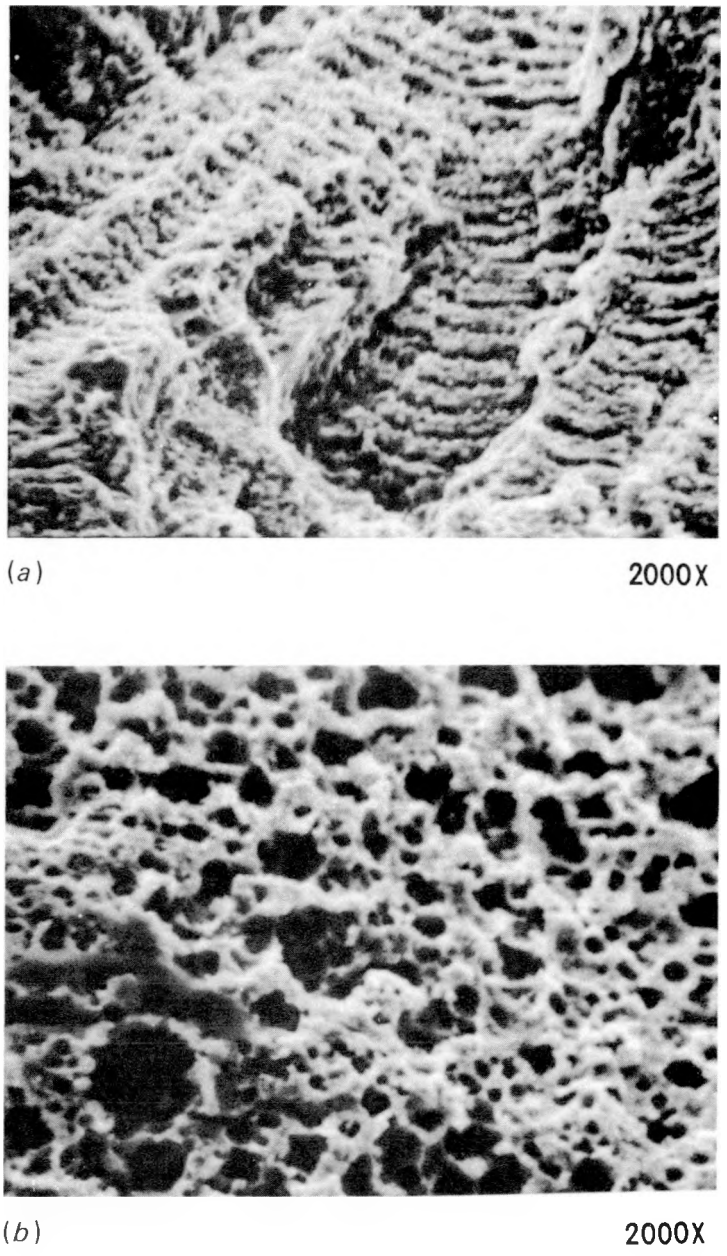

Fig. 3.5. Comparison of fracture surfaces for weld (C-1) and base metal (F-1). (*a*) Specimen F-1, PWR environment, 1 cpm, R = 0.7. (*b*) Specimen C-1, PWR environment, 1 cpm, R = 0.7.

higher density of large carbide particles in the weld metal as shown in Fig. 3.6. Voids form at particle interfaces as a result of plastic strain at the crack tip, and the strain required decreases with increasing particle density.

ORNL PHOTO 1177–78

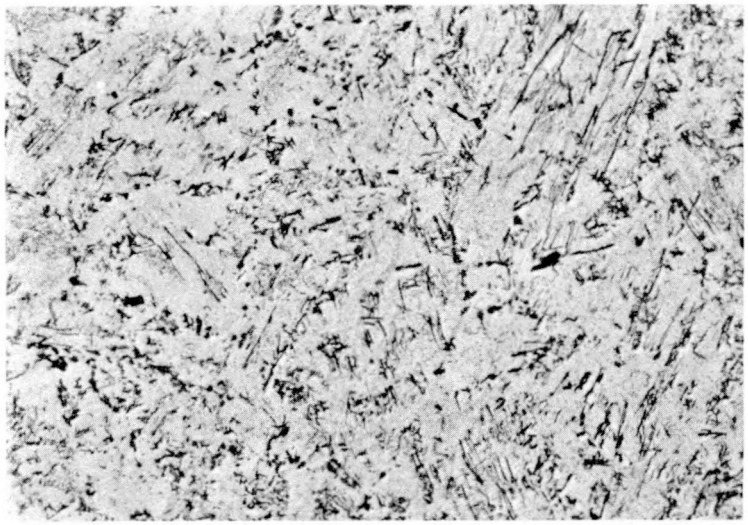

(*a*) 1500X

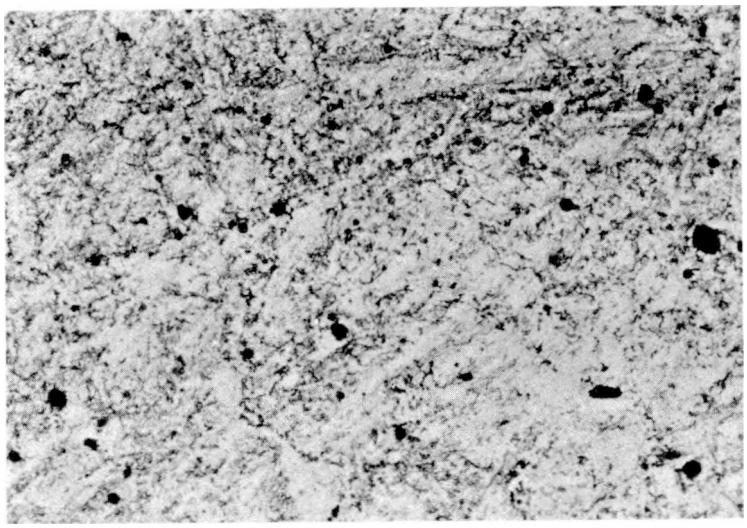

(*b*) 1500X

Fig. 3.6. Extraction replica of carbides in (*a*) base metal specimen 02GB-3 and (*b*) weld metal specimen C-2 showing larger spherical particles in the weld metal.

The influence of hydrogen on the nucleation and growth of microvoids in the plastic zone has been recently reviewed[7] and could include increased nucleation through a decrease in the particle matrix cohesive energy or growth due to a buildup of hydrogen pressure in the void. The enhancement of growth rates in the water environment implies that hydrogen

is able to penetrate the plastic zone to the extent of about the crack opening displacement (COD) during the cyclic test, which is approximately 0.025 μm for an applied stress-intensity factor of 27.5 MPa$\sqrt{m}$. With a diffusion coefficient of 10^{-7} to 10^{-9} cm^2/sec, only 0.06 to 6 sec would be required for hydrogen transport by diffusion; therefore, this does not impose a kinematically limiting effect at the test frequencies imposed (1 cpm imposes a 30-sec rise time). In view of this, it is not surprising that although the microvoid coalescence represents a much different mechanism — it results in a similar crack growth rate.

References

1. G. D. Whitman, *Heavy-Section Steel Technology Program Quart. Prog. Rep. December–February 1977*, ORNL/NUREG/TM-120 (August 1977).
2. W. H. Bamford, D. M. Moon, and L. Ceschini, "Crack Growth Rate Testing in Reactor Pressure Vessel Steels," presented at U.S. NRC Fifth Water Reactor Safety Information Meeting, Gaithersburg, Md., November 1977.
3. G. D. Whitman, *Heavy-Section Steel Technology Program Quart. Prog. Rep. April–June 1977*, ORNL/NUREG/TM-147 (November 1977).
4. T. W. Crooker et al., *Trans. ASM* 61, 568 (1968).
5. A. R. Jack and A. T. Price, *Acta. Met.* 20, 857 (1972).
6. C. E. Richards and T. C. Lindley, *Eng. Fract. Mech.* 4, 951 (1972).
7. A. W. Thompson, *Proceedings of Conference on Environmental Degradation of Engineering Materials Oct. 10–12, 1977*, Virginia Tech., Blacksburg, Va.

4. INVESTIGATIONS OF IRRADIATED MATERIALS*

04397

4.1 Toughness Investigations of Irradiated Materials

R. G. Berggren J. W. Woods
T. N. Jones D. A. Canonico

4.1.1 Second 4T-CTS irradiation study

Impact tests were conducted on 74 Charpy V-notch specimens from the second 4T-CTS irradiation experiment. These specimens were irradiated at temperatures above, below, and near the desired 288°C irradiation temperature. The remaining 110 irradiated Charpy V-notch specimens are being retained for possible future studies.

A summary of the Charpy V-notch impact tests is presented in Table 4.1. A minimum number of specimens were tested in order to retain a maximum number for future studies. From two to seven (average of four) specimens were tested for each combination of fast-neutron fluence and irradiation temperature. Because of the small number of tests, the transition temperatures and temperatures for onset of upper-shelf behavior must be considered approximate. The onset of upper shelf was determined by the "fast load drop method."[1] The fast-neutron fluences are approximate since final dosimetry results are not yet available.

All tests show radiation-induced increases of Charpy transition and onset of upper-shelf temperatures and decreases of ductile (upper shelf) fracture energy and lateral expansion for average irradiation temperatures as high as 345°C. Specimens of weldment 61W that had been irradiated to fluences of 3 to 13 $\times 10^{18}$ neutrons/cm^2 (E > 1 MeV) at average temperatures of 295 to 345°C showed transition temperature increases of 30 to 80 K and ductile fracture energies of 68 to 76 J (unirradiated ductile fracture energy was 84 J). Specimens of weldment 62W, irradiated to fluences of 6 to 16 $\times 10^{18}$ neutrons/cm^2 (E > 1 MeV) at average temperatures of 299 to 313°C, showed transition temperature increases of

---

*Conversions from SI to English units for all SI quantities are listed on a foldout page at the end of this report.

Table 4.1. Charpy V-notch impact test results from second 4T-CT irradiation experiment[a]

Fluence[b] (E > 1 MeV) (neutrons/cm^2)	Irradiation temperature (°C)		Transition temperature[c] (°C)	Onset of upper shelf[c] (°C)	Upper-shelf energy (J)	Upper-shelf lateral expansion [mm (0.001 in.)]
	Forward	Reverse				
			Weldment 61W, capsule A			
0			−18	40	84	1.52 (60)
3×10^{18}	330	360	10	60	76	1.27 (50)
3×10^{18}	320	330	40	75	73	1.27 (50)
6×10^{18}	330	335	25	65	73	1.27 (50)
6×10^{18}	305	320	30	65	76	1.02 (40)
13×10^{18}	310	310	60	90	68	1.14 (45)
9×10^{18}	295	295	50	85	70	1.07 (42)
			Weldment 62W, capsule B			
0			−9	40	91	1.65 (65)
14×10^{18}	315	305	40	80	76	1.40 (55)
16×10^{18}	280	315	50	90	76	1.27 (50)
6×10^{18}	305	305	25	70	81	1.32 (52)
13×10^{18}	290	305	50	70	79	1.27 (50)
9×10^{18}	250	280			73	1.27 (50)
9×10^{18}	275	255	60		73	1.27 (50)
6×10^{18}	255	305	50	90	84	1.22 (48)
			Weldment 63W, capsule C			
0			−23	40	88	1.60 (63)
12×10^{18}	320	320	70	110	65	1.14 (45)
10×10^{18}	320	310	60	95	68	1.14 (45)
6×10^{18}	290	340	60	95	70	1.14 (45)
10×10^{18}	285	335	80	120	68	1.07 (42)
6×10^{18}	315	290	75	95	68	1.02 (40)
9×10^{18}	280	280	90	110	68	0.97 (38)

[a] All temperatures except the average transition temperatures for unirradiated control specimens are rounded to the nearest 5°C.

[b] Estimated fast-neutron fluences.

[c] Approximate values based on a minimum number of tests.

39 to 61 K and ductile fracture energies of 76 to 81 J (unirradiated ductile fracture energy was 91 J). Specimens of the same weldment irradiated to 9×10^{18} neutrons/cm^2 (E > 1 MeV) at an average temperature of 280°C showed a transition temperature increase of 58 K and a ductile fracture energy of 84 J. Specimens of weldment 63W irradiated to fluences of 6 to 12×10^{18} neutrons/cm^2 (E > 1 MeV) at an average temperature of 280 to 321°C showed transition temperature increases of 83 to 111 K and ductile fracture energies of 65 to 70 J (ductile fracture energy of unirradiated material was 88 J).

4.1.2 Third 4T-CTS irradiation study

Irradiation of the third 4T-CTS irradiation experiment was started in December, and the first rotation of the three capsules is scheduled in January. These capsules contain additional weldment specimens.

(38-40) 04398

4.2 J_{Ic} Values of Irradiated ASTM A533, Grade B, Class 1, Steel at 177°C*

J. A. Williams†

The J_{Ic} fracture toughness of ASTM A533 grade B, class 1, steel irradiated to 2.5 to 2.7×10^{19} neutrons/cm^2 at 290°C was determined using 10-mm-thick compact specimens. At the test temperature of 177°C, it was expected that fully ductile behavior would be exhibited during fracture testing.

The methodology currently being developed by ASTM[2,3] was used as test guidance. Heat tinting was used to distinguish stable crack extensions, and measurements were made at nine equally spaced intervals along the crack fronts to determine the initial and final crack lengths. The J-integral was calculated by the Merkle-Corten[4] equation for the compact specimen.

---

*Research performed under Purchase Order 11Y-50917V for the Oak Ridge National Laboratory, operated by Union Carbide Corporation under contract to the U.S. Energy Research and Development Administration (now DOE).

†Hanford Engineering Development Laboratory.

A linear regression analysis of the J vs Δa data was used to determine the R curve and the intersection value J_{Ic} of the R curve with the blunting line.

The data for all specimens are given in Table 4.2. The R curve is shown in Fig. 4.1 for the irradiated A533-B1 together with the R curve determined for unirradiated A533-B1 specimens up to 101.6 mm in thickness.[5] Both irradiated and unirradiated material were in the TL orientation.

Table 4.2. R-curve data for irradiated ASTM A533-B1, TL orientation, tested at 177°C

Specimen	Size (mm)	a (mm)	a/w	J (kJ/m^2)	Δa (mm)
W58-56	10.0	11.68	0.584	29	0.000
W58-54	10.0	12.01	0.600	54	0.051
W58-53	10.0	12.01	0.600	118	0.178
W58-51[a]	10.0	11.91	0.595	186	0.254
W58-52[a]	10.0	12.01	0.600	278	0.762
W58-55[a]	10.0	11.84	0.591	428	1.448

[a]Specimens used in linear regression analysis to establish R curve of Fig. 4.1.

Yield strengths,[5,6] ultimate strengths,[6] and C_V shelf energies[7] are given for irradiated and unirradiated material in Table 4.3.

The J_{Ic} toughness of the irradiated A533-B1 was determined to be 155 kJ/m^2 as compared to 349 kJ/m^2 prior to irradiation. Thus, the reduction in upper-shelf J_{Ic} toughness is approximately 55%; C_V energy on the upper shelf is observed from Table 4.3 to be reduced by only 13%.

Only the closest point to the blunting line on the irradiated material R curve meets all the requirements of size and Δa interpretation range for establishing J_{Ic} and the R curve.[2,3] Thus, the J_{Ic} value determined should be considered as preliminary. It would also be expected that the R-curve slope of irradiated material might be less than that of unirradiated material; this is not the case, suggesting that the specimens used for the R-curve analysis were too small.

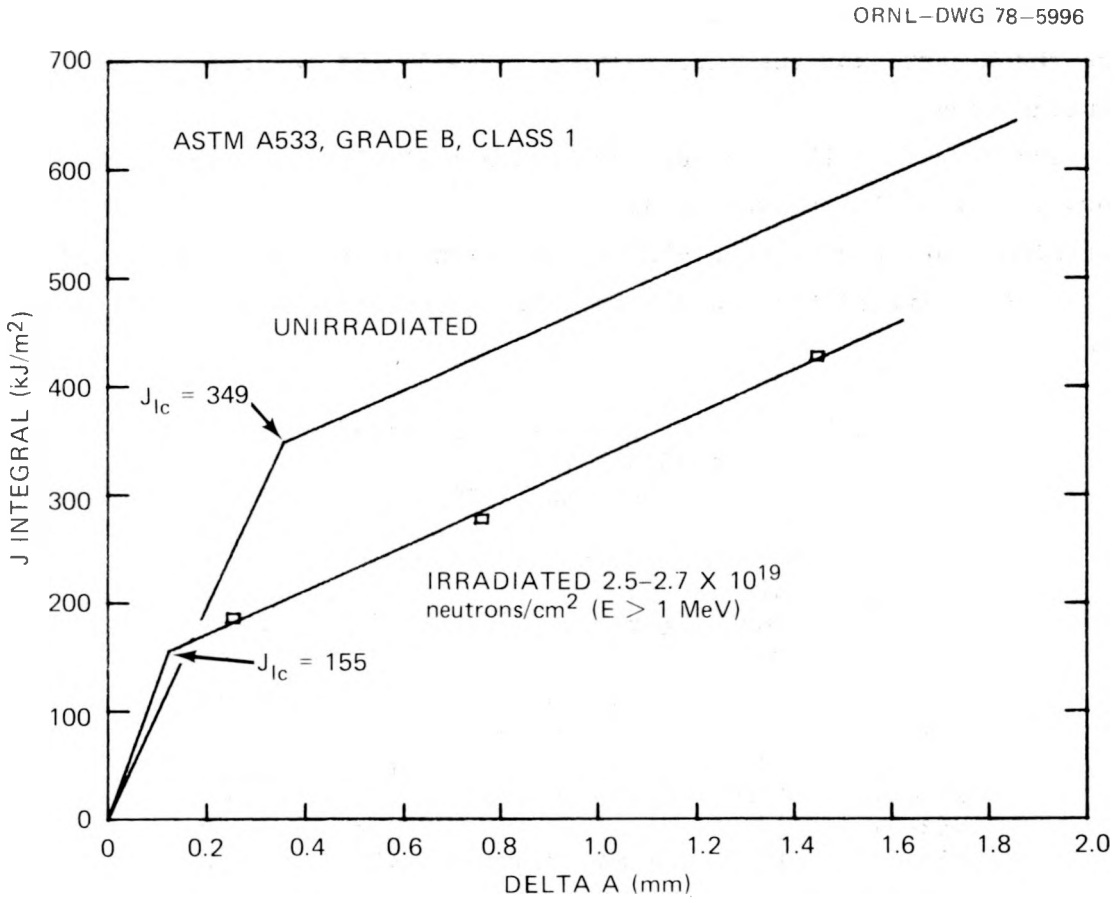

Fig. 4.1. R curve for A533 unirradiated material tested at 121°C and irradiated material tested at 177°C.

Table 4.3. Mechanical properties of ASTM A533, grade B, class 1 steel[a]

	Unirradiated[a]	Irradiated[b]
Yield strength, MPa	420	572
Ultimate strength, MPa	558	689
C_V energy, J	126	110

[a]Properties for test temperature of 121°C.

[b]Properties for test temperature of 177°C; irradiated 2.5 to 2.7 × 10^{19} neutrons/cm^2 (E > 1 MeV) at 290°C.

4.3 Evaluation of the Unloading Compliance Technique for Single Specimen J Integral Testing*

G. A. Clarke† J. D. Landes†

A contract was recently signed by Westinghouse R&D Center and Oak Ridge National Laboratory for the evaluation of the unloading compliance technique as presently used in single-specimen J-integral tests. The principal objective of this program is to develop a methodology for testing that is accurate, repeatable, and fully applicable to hot-cell J-integral testing of pressure vessel steels. The program consists of three major project areas: (1) Present System Evaluation and Improvements, (2) Sensitivity and Reproducibility Studies, and (3) Procedure Verification Tests.

4.3.1 Project progress report

A computer program has recently been completed which allows a data acquisition system to accept load and displacement voltages from the test. These voltage values are used to calculate the area under the load-displacement curve along with the unloading compliance from the periodic unloadings made during the test. From these area and unloading compliance values, the value of J and crack extension is calculated and plotted by a plotting routine attached to the computer. Initial tests to check out this program are presently under way.

Evaluations of extraneous electronic and mechanical noises that may well affect the accuracy and the repeatability of the tests have been made. This resulted in the replacement of a high-rate servohydraulic valve with a MOOG-type valve. The noise resulting from the high-rate valve gave unacceptable noise levels in the load signal. An evaluation is presently under way to determine the difference in amounts of friction between clevises with bearings and a clevis with flat bottom holes. A flat bottom hole clevis has been manufactured with ceramic inserts, which

---

* Work sponsored by HSST Program under UCCND Subcontract 7394 between Union Carbide Corporation and Westinghouse Electric Corporation.

† Westinghouse Electric Corporation.

should remove the effects of brinneling by the loading pins. A test matrix was developed to investigate various clevis arrangements and load point displacement measurement techniques in order to reduce the hysteresis in the unloading slopes of the load-displacement records. The specimens to be used for these tests are blunt-notch compact specimens. These specimens provide the added advantage of evaluating various rotation correction factors presently being used to correct the compliance values due to the rotation of load and displacement measuring points.

4.3.2 Outline of future work

A series of tests on blunt-notch specimens is planned to determine the sensitivity attainable in J-integral tests of compact specimens ranging from 1/2T to 4T. Once this level of sensitivity has been determined and compared to the practical degree of sensitivity required, tests are planned to complete a full set of J vs Δa R curves on A508 material. A confirmation set of tests on the same material is to be run by Westinghouse Hanford in order to determine the reproducibility of these tests. Tests are also planned for an A533 material with an upper-shelf Charpy energy of 95 J. This activity will be performed in close cooperation with Westinghouse Hanford Engineering Development Laboratory in order to develop a test methodology for hot-cell testing. Continued technical communication with various other research groups active in J-integral testing will remain a high priority throughout the program. It is planned that at the completion of this contract a demonstrated and accepted approach to single-specimen testing will be ready for use under irradiated conditions.

References

1. D. A. Canonico et al., *Use of Instrumented Charpy Tests to Determine Onset of Upper Shelf Energy*, ORNL-5086 (November 1975).
2. "Plane Strain Fracture Toughness of Metallic Materials," ASTM E399-72, *Annual Book of ASTM Standards*, Part 31, American Society for Testing and Materials, Philadelphia, Pa.
3. G. A. Clarke, "Recommended Procedure for J_{Ic} Determination," presented at the ASTM E24.01.09 Task Group Meeting, Norfolk, Va., March 1977.

4. J. G. Merkle and H. T. Corten, "A J-Integral Analysis for the Compact Specimen, Considering Axial Force as Well as Bending Effects," *ASME Transactions, Journal of Pressure Vessel Technology* (November 1974).

5. J. A. Williams, *The Irradiation and Temperature Dependence of Tensile and Fracture Properties of ASTM A533, Grade B, Class 1 Steel Plate and Weldment*, HSSTP-TR-31, HEDL TME 73-75 (August 1973).

6. J. A. Williams, "Strain Rate-Temperature Parameterization of Irradiated and Unirradiated Yield Strength of A533-B Plate and Weld and A508 Forging," *Heavy-Section Steel Technology Program Quart. Prog. Rep. April–June 1975*, ORNL/TM-5021, Vol. II (September 1975).

7. R. G. Berggren and T. N. Jones, "Toughness Investigation of Irradiated Materials," *Heavy-Section Steel Technology Program Quart. Prog. Rep. July–September 1974*, ORNL/TM-4729, Vol. II (November 1974).

5. PRESSURE VESSEL INVESTIGATIONS*

5.1 Trial Preparation of V-8 Type Flaw

P. P. Holz

The test of vessel V-8 calls for an axially oriented outside-surface flaw to be placed in a region of high residual stress and low toughness near a half-bead weld repair.[1,2] It appears that a flaw placed in the original fabrication submerged-arc weld near the repair weld will produce an optimum combination of high residual stress and low toughness for a transition temperature test.

Procedures and equipment for machining and sharpening the V-8 flaw were tried on a cylindrical remnant of the fractured vessel V-9. A notch of the desired contour for the V-8 test was milled into the longitudinal submerged-arc weld of the V-9 cylinder. The apparatus that will be used for fatigue sharpening the V-8 flaw was used to sharpen the prototype.

The V-9 cylinder was placed vertically onto a 127-mm mill table bed to generate a typical V-1-type semicircular notch 206 mm long at the surface of the cylinder by 50.8 mm deep, as shown in Fig. 5.1. The contour of the notch tip was circular at the two ends joined by a straight section about 30 mm long at the deepest part of the notch. A number of slitting saws were used. The final cutter was ground to a 30° included angle with a 0.127- to 0.191-mm tip radius so as to give the tip of the notch a sharp point. A flat plane was also milled onto the vessel surface perpendicular to the flaw slot to establish a precision surface on which to mount a block for sealing the notch for pressurization. After the machining operation was completed, a silastic rubber impression of the cavity was made, and a stainless steel insert was fabricated from the rubber mold to obtain a tight-fitting plug (0.04 mm maximum clearance). The insert provided side grooves to channel hydraulic oil to and from the bottom of the notch.

---

*Conversions from SI to English units for all SI quantities are listed on a foldout page at the end of this report.

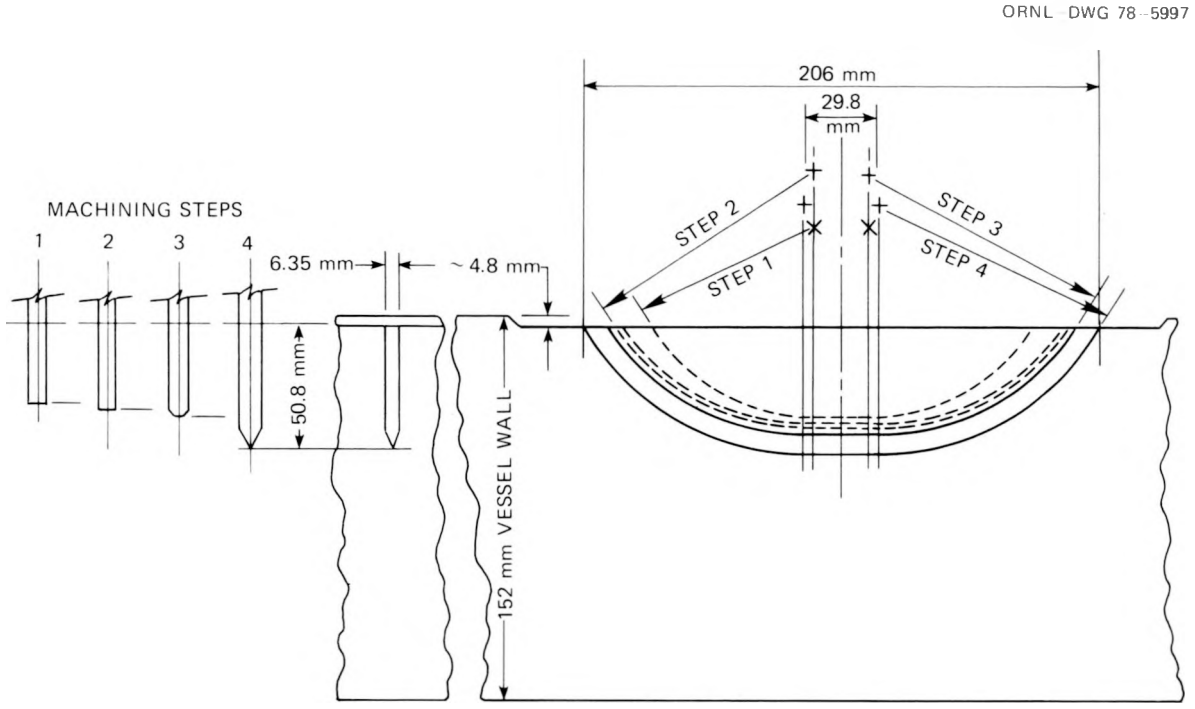

Fig. 5.1. Proposed flaw and machining sequence for V-8 test.

The seal-block and clamp-ring setup previously used for cyclic pressurization of flaws[3] was reactivated and installed on the notched cylinder as shown in Fig. 5.2. The two original clamping rings wrapped completely around the test vessels. This arrangement on the V-9 remnant, which was split, did not permit satisfactory tightening of the seal block. The rings were cut, and the four ends of the partial rings were then welded directly to the cylinder at points about 100° from the flaw. The notch was pressurized cyclically with an Aminco 138-MPa pump delivering 1 cycle/stroke at a rate of 30 to 35 strokes/min. Maximum pressure was regulated to about 114 MPa. Flaw growth was monitored by shear wave ultrasonic transducers mounted on the inside surface of the cylinder. Fatiguing was stopped when the flaw growth at the center of the notch was indicated ultrasonically to be about 13 mm. This occurred at 106,000 pressure cycles. No difficulties were encountered with the "O"-ring-sealed clamping block or the pumping equipment.

Upon removal of the clamping block, flaw growth at the outer surface was verified visually, as shown in Fig. 5.3. The flaw was cut from

ORNL PHOTO 1178–78

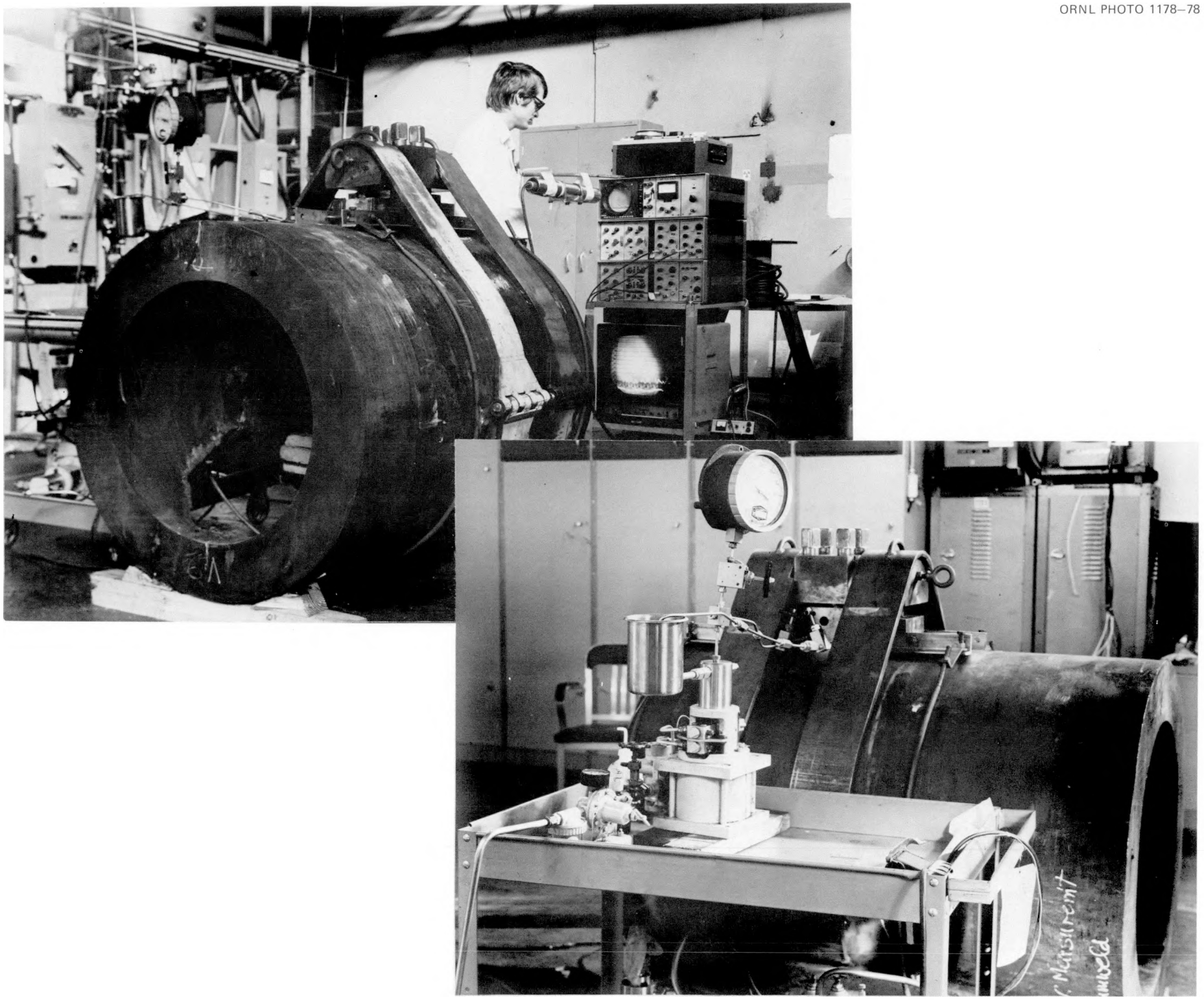

Fig. 5.2. Hydraulic flaw-fatiguing setup for V-8 prototype flaw sharpening.

ORNL PHOTO 1179–78

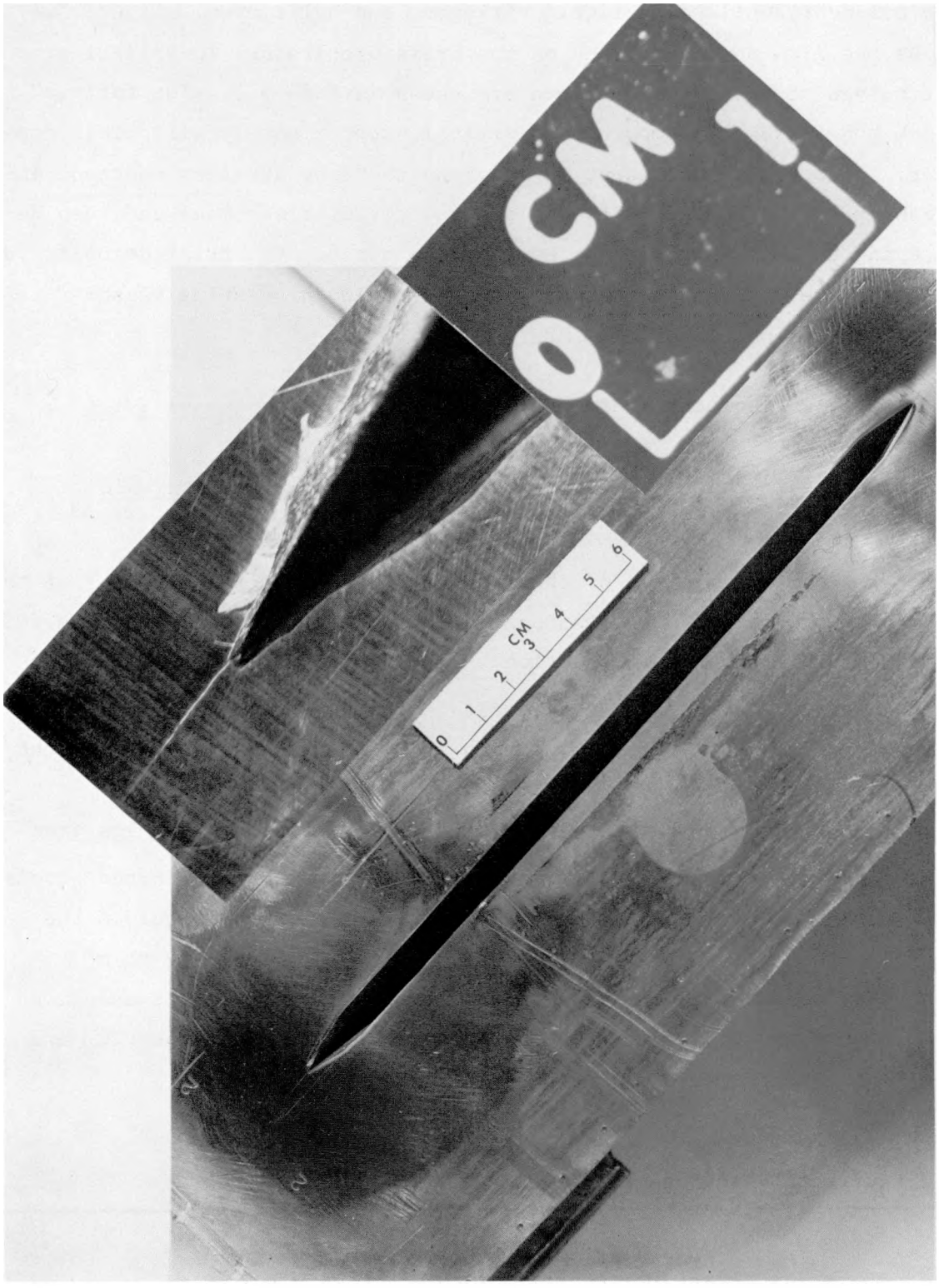

Fig. 5.3. V-8 prototype flaw specimen, outside surface views.

the cylinder, chilled in liquid nitrogen, and split open. Figure 5.4 shows the flaw specimen block on the press preparatory to splitting. The halves of the split specimen are shown in Fig. 5.5. The fatigue crack had grown to a smooth, symmetrical, approximately elliptical contour. Flaw growth was about 12 mm along the deep straight section, increasing to about 18 mm midway along the circular sections and then decreasing to about 6 mm at the ends of the notch. The trial demonstrated that the equipment and procedures are suitable for flawing vessel V-8.

5.2 Characterization of the Repair Weld in Vessel V-8

5.2.1 Fracture toughness investigations of the fabrication weld (W. J. Stelzman, D. A. Canonico)

The characterization of the static fracture toughness (K_{Icd}) of the V-8 fabrication weld metal was continued using 2T compact specimens (CS) machined from the V-9 prolongation. The location of the two specimens in the weld, together with the results obtained from each specimen, is shown in Fig. 5.6. Crack propagation is in the welding direction; the specimen is WL oriented.

A comparison of the results from the 2T CS with the results from precracked Charpy specimens (PCC_V) and 1T CS previously reported[4] indicates that the transition from low to high toughness behavior in the larger specimen occurs at a higher temperature. At the 110-$MN \cdot m^{-3/2}$ toughness level, the mean K_{Icd} value from the two 2T compact specimen occurs at about −15°C, whereas the mean K_{Icd} values from the PCC_V and the 1T CS occur at −38 and −26°C, respectively.

5.2.2 Fracture toughness of the qualification weld (W. J. Stelzman, D. A. Canonico)

The static fracture toughness of the 44-mm-thick weld qualification test plate 01MS-C1 described previously[5] was continued using precracked Charpy-V (PCC_V) and 1T compact specimens. All the specimens were WL

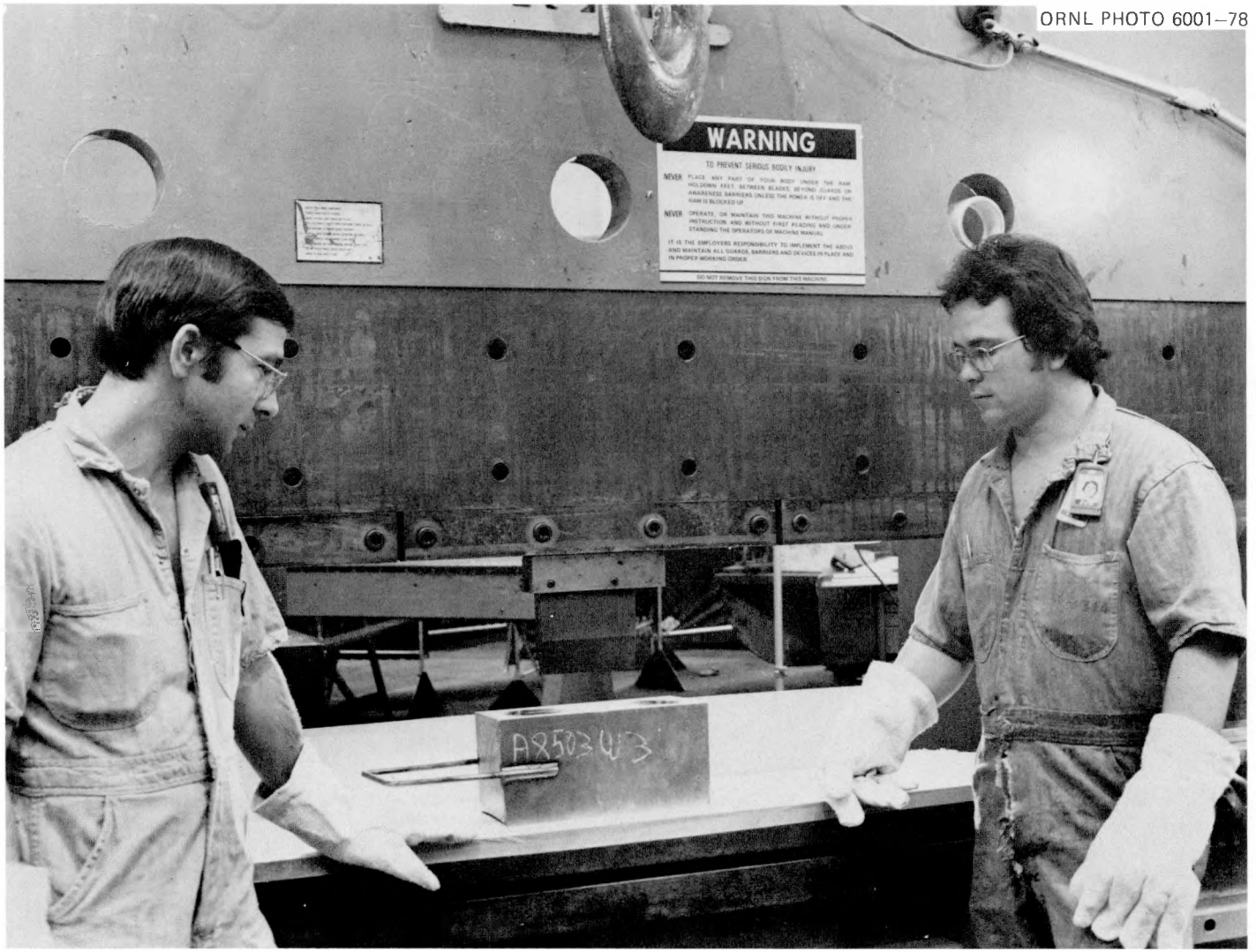

Fig. 5.4. V-8 prototype flaw specimen on press prior to splitting.

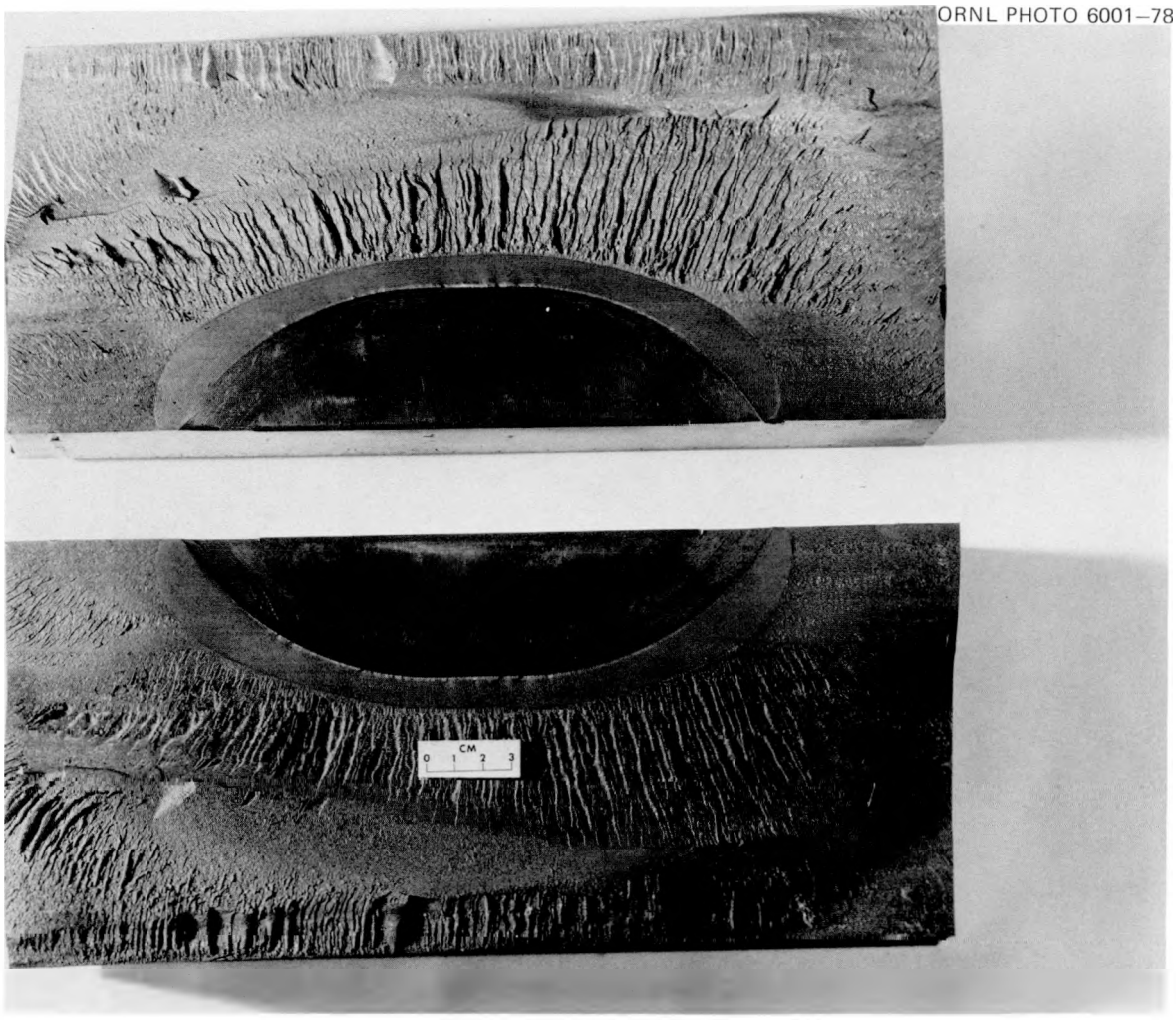

Fig. 5.5. Split halves of V-8 prototype flaw.

oriented in the weld metal with the fatigue precrack on the centerline of the weldment.

Test results are listed in Table 5.1 and are plotted in Fig. 5.7. The K_{Icd} toughness of the weld metal from the PCC_V specimens is dependent on the depth in the weld from which the specimens were obtained. Lower values were noted for midthickness specimens for a given test temperature than for specimens from the quarter- and three-quarter depth levels. The maximum K_{Icd} value, 303 $MN \cdot m^{-3/2}$, occurred at 37.8°C at the quarter (and three-quarter) level. Higher toughness values may occur at the midthickness, at temperatures above 24°C, but no tests were made at these higher temperatures.

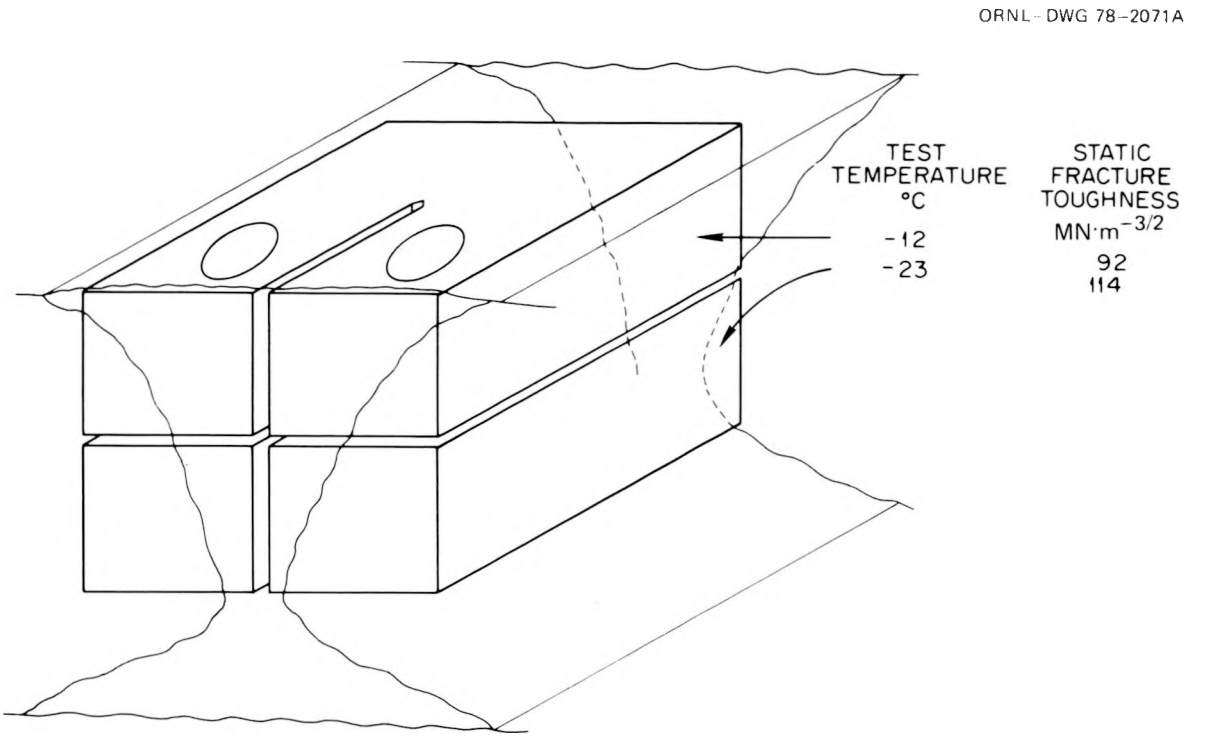

Fig. 5.6. Layout and test results from the 2T compact tension specimens from the vessel fabrication weld in the V-9 prolongation.

Table 5.1. Precracked Charpy-V and 1T compact specimen fracture toughness at various depths in the qualification test plate 01MS-C1

Temperature (°C)	Static fracture toughness (MN·m$^{-3/2}$)	
	PCC_V	1T CS
	Quarter thickness	
−73.3	213	
37.8	303	
149	203	
	Midthickness	
−45.6	111	114
−17.8		129
65.6	235	
	Three-quarter thickness	
−17.8	268	
93.3	262	
204	179	

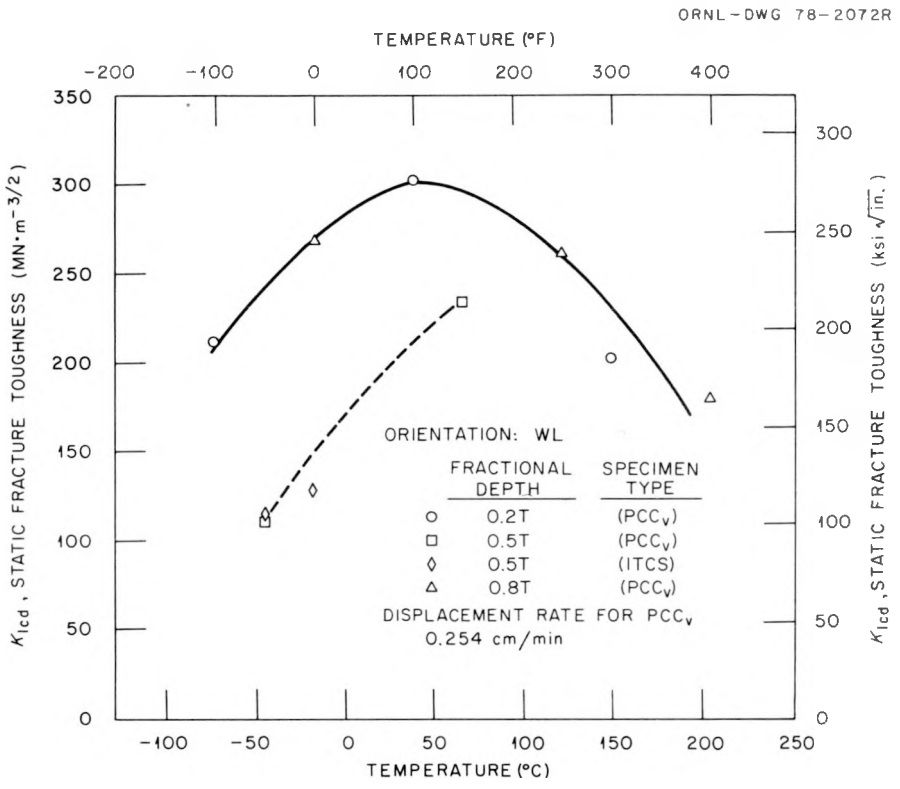

Fig. 5.7. Variation of static fracture toughness with temperature for 44-mm-thick 1/2-bead technique qualification weldment 4W.

The 1T compact specimen results correlate very well with the limited PCC_V results at the same depth level (midthickness).

5.2.3 Fractographic examination of ITV-8 fabrication weld (D. A. Canonico, R. S. Crouse)

The results of the previously reported[5] scanning electron microscopy (SEM) studies of the precracked Charpy V-notch (PCC_V) specimens showed a relationship between fracture toughness and amount of dimple fracture at the fatigue crack tip. This is the site of initial crack extension in the PCC_V test. This behavior suggested a relationship between the microstructure at the fatigue crack tip and the fracture toughness exhibited by the PCC_V specimen. It was found during testing of the fabrication weld from the V-9 prolongation that both tough and frangible behavior was exhibited by the weld metal at −46°C. The data that were previously reported are shown in Fig. 5.8. Note that at −46°C the PCC_V toughness

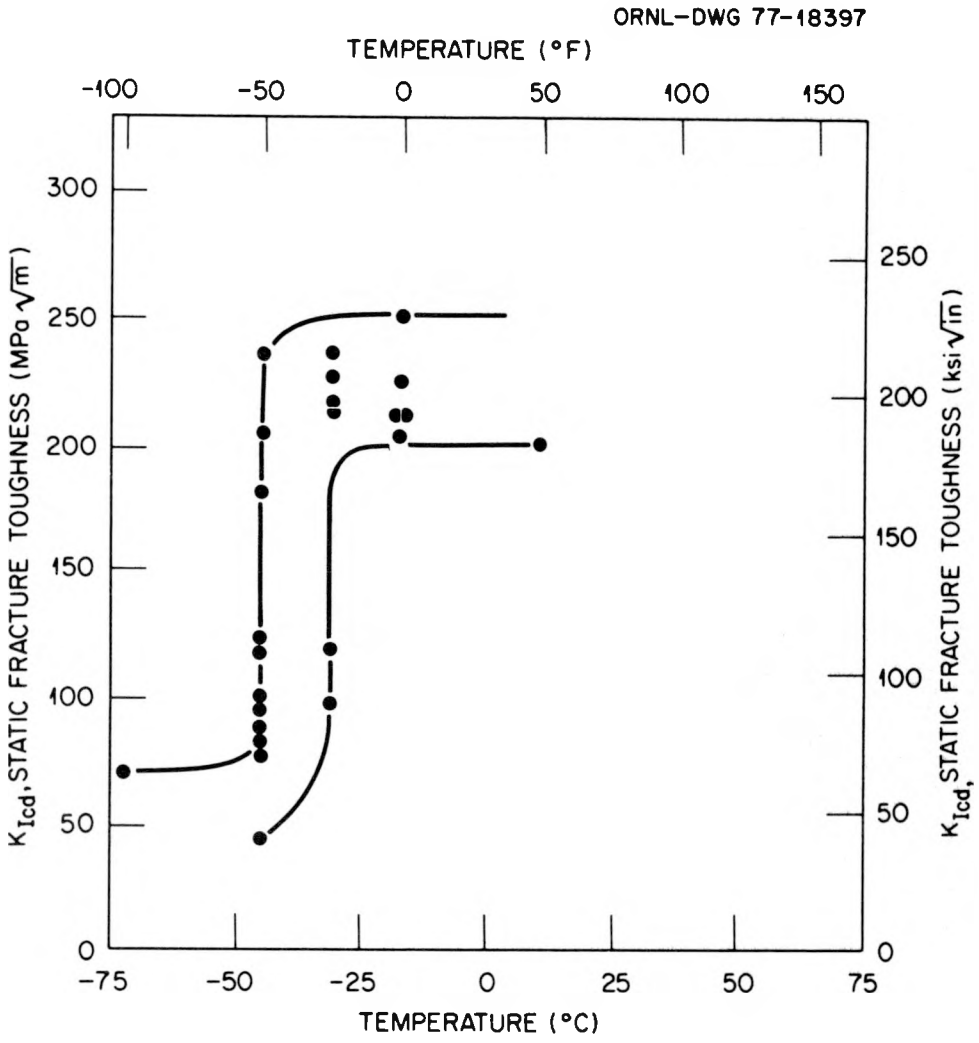

Fig. 5.8. Precracked Charpy static fracture toughness results from the vessel fabrication weld metal in the V-8 prolongation.

values ranged from about 44 to 236 $MN \cdot m^{-3/2}$. One contention is that the reason for the wide spread in PCC_V toughness in the weld metal is due to the size of the Charpy specimen (10 mm square) in relation to the size of the weld nugget. A nearly full-size photograph of an etched section of the V-9 prolongation fabrication weld is shown in Fig. 5.9. Superimposed on the photograph is the outline of the cross section of a Charpy V-notch specimen. It is evident that the PCC_V specimen is somewhat smaller in width than the individual weld passes. This suggests that the PCC_V toughness properties will be affected by the location of the individual Charpy specimens relative to the columnar (as deposited) weld

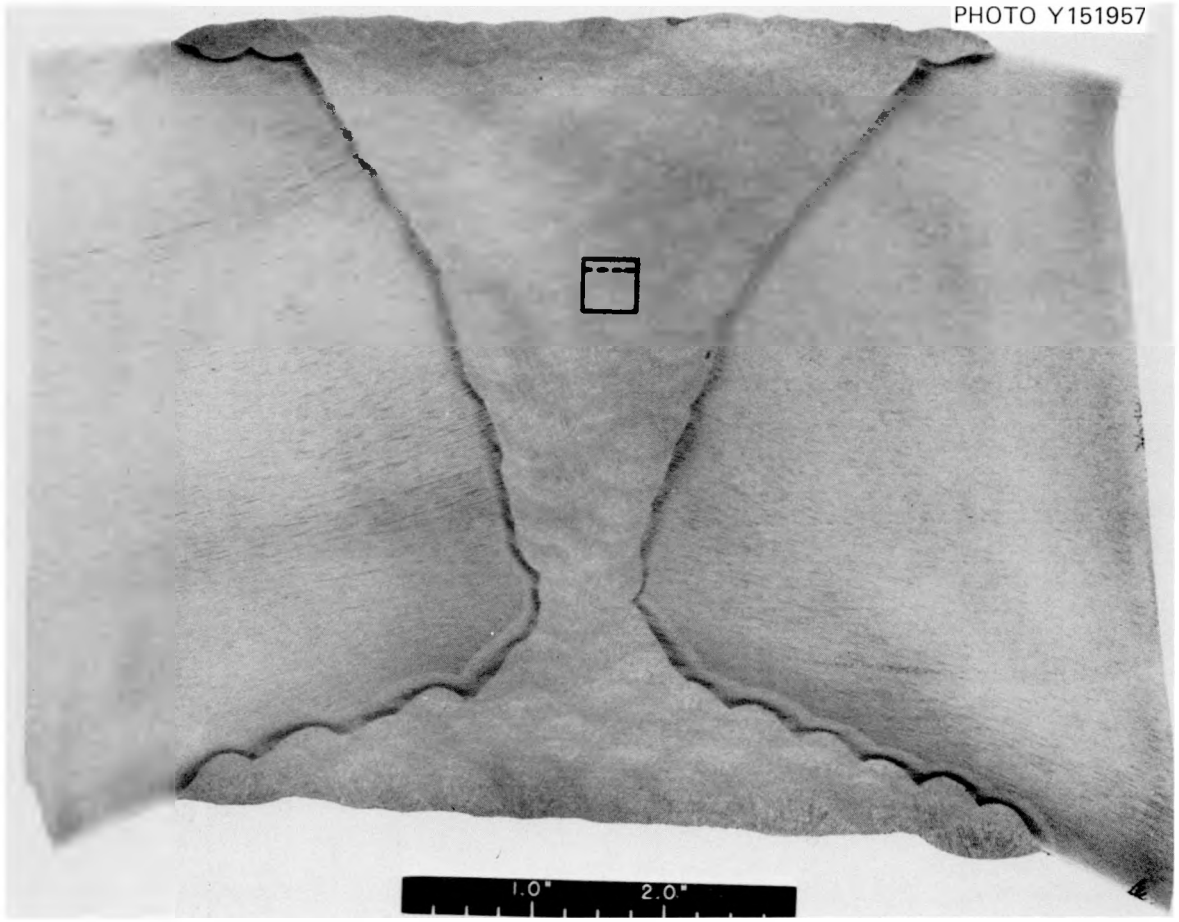

Fig. 5.9. Photomacrograph of fabrication weld in V-9 prolongation. A Charpy specimen is superimposed on the weld metal to show the relationship between its size and the size of the individual weld passes. Original reduced 16%.

metal structure and refined weld metal structure (that region of a weld pass that is reaustenitized as a consequence of subsequent passes).

We undertook an SEM–light microscopy study to determine whether or not our explanation for the wide range in PCC_V properties was correct. For that study we selected PCC_V specimens that were tested at −46°C and exhibited frangible behavior (specimen V8W73) and tough behavior (specimen V8W70). The fracture toughness values exhibited by these specimens are listed in Table 5.2. The fracture surfaces from these specimens were examined in the SEM, and the fracture mode at the bottom of the fatigue crack was determined. Next, the specimens were sectioned and metallographically polished in order to examine the cross section of

Table 5.2. Static fracture toughness properties of the fabrication weld precracked Charpy V-notch specimens metallographically examined

Specimen No.	Test temperature (°C)	Static fracture toughness, K_{Icd} ($MN \cdot m^{-3/2}$)
V8W73	−46	79
V8W70	−46	181
V8W57	−46	82
V8W76	−46	96
V8W58	−46	44
V8W55	−46	204
V8W69	−73	70
V8W74	−18	225

the fracture tip (i.e., the cut was perpendicular to the fracture propagation path). Both 25× and 500× photomicrographs were taken of the microstructure at the crack tip. Figure 5.10 contains the results of the metallographic examination of the fatigue crack tip region of a PCC_V specimen (V8W73) that failed in a brittle mode. Note that the tip of the fatigue crack resides in a weld region that contains coarse columnar grains. This specimen exhibited frangible behavior at −46°C. The crack initiation region of this specimen contained a very narrow band of dimple fracture mode at a magnification of 1000× in the SEM.

PCC_V specimen V8W70 was selected for the metallographic study of a high-toughness specimen tested at −46°C. This specimen exhibited a K_{Icd} toughness of 181 $MN \cdot m^{-3/2}$ at −46°C. The PCC_V fatigue crack tip in this specimen, shown in Fig. 5.11, resided in a region of the weld metal whose microstructure had undergone refinement due to subsequent weld passes. This microstructure exhibited tough behavior at −46°C, as reflected in the dimple fracture mode seen at the crack tip in the SEM study.

These two specimens, V8W73 and V8W70, are used in this report to illustrate the relationship between the site of the PCC_V fatigue crack tip and the microstructure of the weld passes. Similar studies were completed on the other specimens listed in Table 5.2, and the results

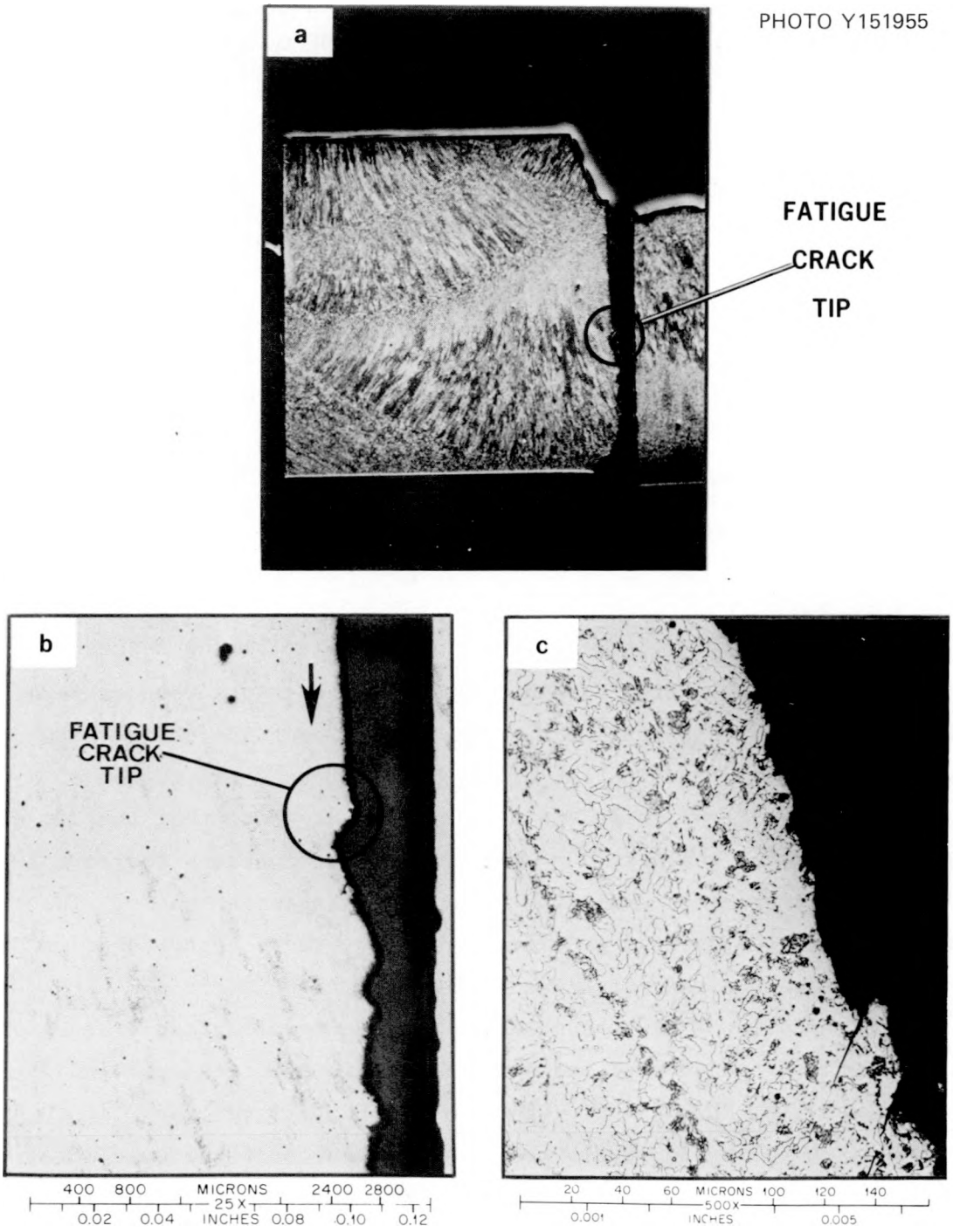

Fig. 5.10. Metallographic examination of the fatigue crack tip area from PCC_V specimen V8W73. This specimen was tested at −46°C and exhibited a fracture toughness of 79 $MN \cdot m^{-3/2}$. (*a*) is a photomacrograph showing the location of the fatigue crack tip in relation to the weld passes, (*b*) shows the coarse columnar grains at the crack tip, and (*c*) shows the microstructure at the crack initiation site. Original reduced 15%.

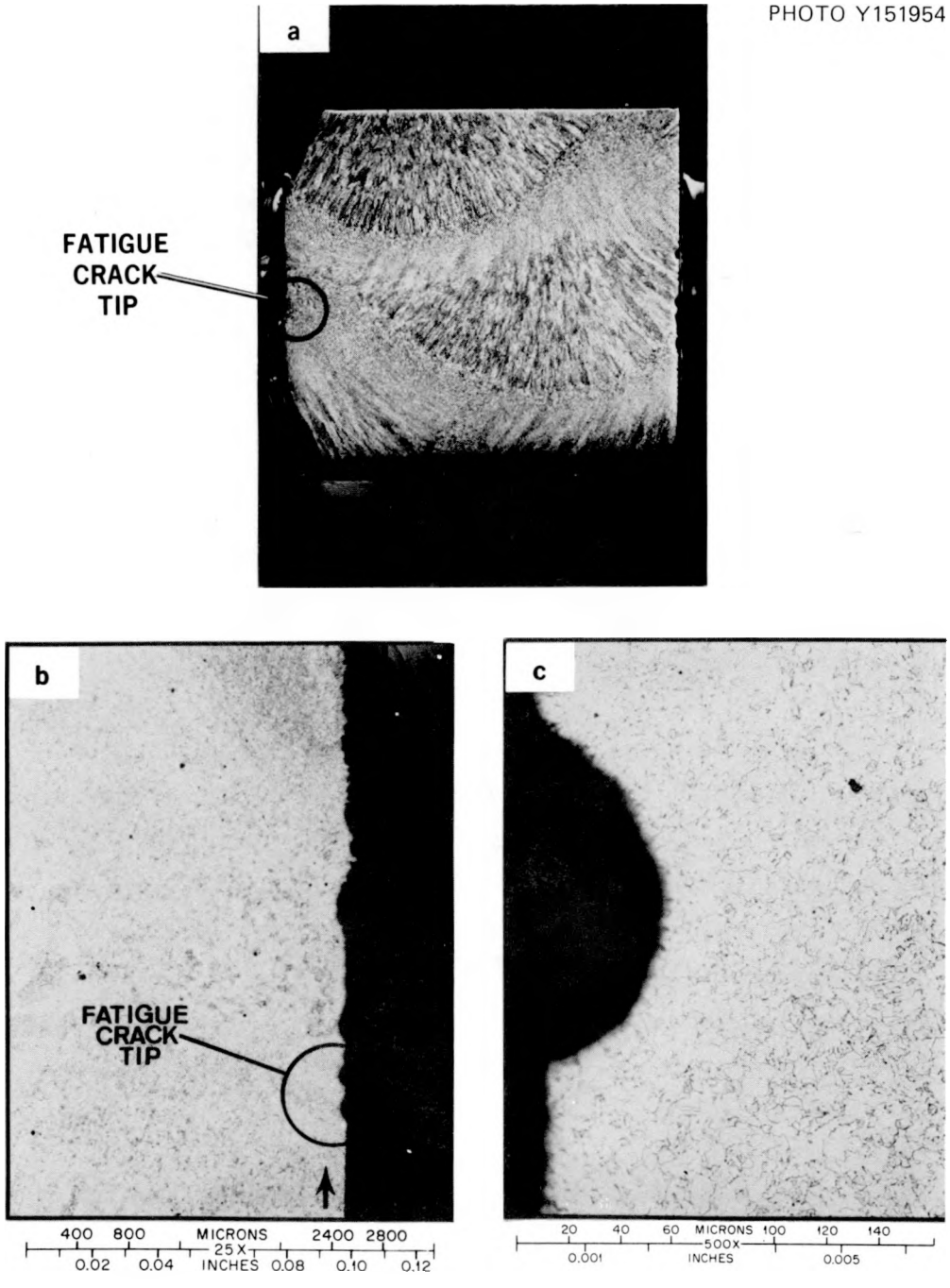

Fig. 5.11. Metallographic examination of the fatigue crack tip area from PCC_V specimen V8W70. This specimen was tested at −46°C and exhibited a fracture toughness of 181 $MN \cdot m^{-3/2}$. (*a*) is a photomacrograph showing the location of the crack tip in relation to the weld passes, (*b*) shows that the crack tip resides in a region that contains a refined microstructure (a microstructure that underwent reaustenitization due to subsequent weld passes), and (*c*) is a photomicrograph of the microstructure at the crack initiation site. Original reduced 18%.

were nearly identical to those shown in Figs. 5.10 and 5.11; that is, specimens tested at −46°C exhibited low PCC_V toughness values (below 110 $MN \cdot m^{-3/2}$) if their fatigue crack tips resided in the columnar (not reaustenitized) grain region of the individual weld passes. These results suggest that the ductile to brittle transition temperature for the refined weld metal microstructures lies below −46°C and the transition temperature for the coarse columnar grains lies above −46°C.

To determine the validity of this hypothesis, we examined PCC_V specimens tested at −73 and −18°C. Figure 5.12 contains the results of the metallographic study of the PCC_V specimen (V8W69) which was tested at −73°C. It is evident in Fig. 5.12*a* that the fatigue crack tip resides in an area of the weld metal microstructure that was refined as a consequence of simultaneous weld passes. Regardless of the fact that the crack tip resided in refined microstructure, this specimen exhibited a low fracture toughness (70 $MN \cdot m^{-3/2}$). This result is substantiated in the SEM examination of the fracture at the crack initiation site. The fatigue crack tip region exhibited essentially all cleavage mode even when viewed at a magnification of 1000×, suggesting that the transition temperature of the refined weld metal microstructure is −73°C or higher.

The metallographic investigation was completed by examining a PCC_V specimen that was tested at −18°C and that had exhibited excellent toughness. PCC_V specimen V8W74, with a K_{Icd} of 225 $MN \cdot m^{-3/2}$ at −18°C, was selected for this study. Figure 5.13 contains the results of this study. The fatigue crack tip resides in the coarse columnar-grained region of the weld. This can be seen in Fig. 5.13*a*; the coarse grains are explicitly shown in Fig. 5.13*b*. Despite the fact that the fatigue crack tip resided in a region of coarse columnar grains, the fracture toughness was exceedingly high. This result shows that the transition temperature of the coarse columnar grains is −18°C or below but not at −46°C.

As a result of this study we have concluded that the wide range of toughness values obtained with PCC_V specimens at the transition temperature is due to the location of the fatigue crack tip. The heterogeneous microstructure of the individual weld passes in a high heat input weld produced by the submerged-arc process (or any other welding process if high heat inputs are employed) is due to the partial refinement of previous

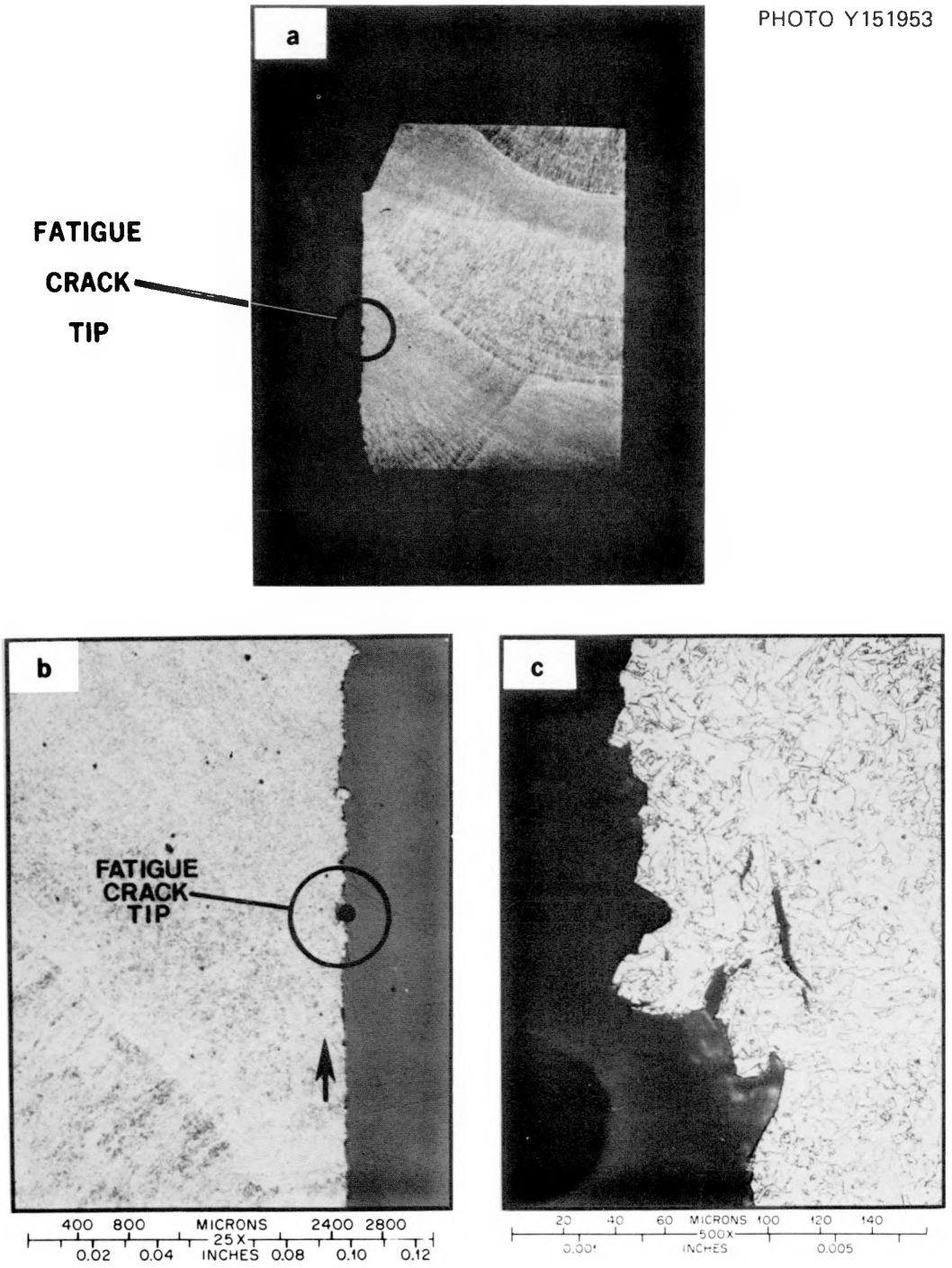

Fig. 5.12. Metallographic examination of the crack tip region of PCC_V specimen V8W69. This specimen was tested at −73°C and exhibited a fracture toughness of 70 $MN \cdot m^{-3/2}$. The crack tip resides in the refined region of the weld metal microstructure as shown in (*a*) at the magnification of 25×. The microstructure in this region is shown in (*b*). Original reduced 15%.

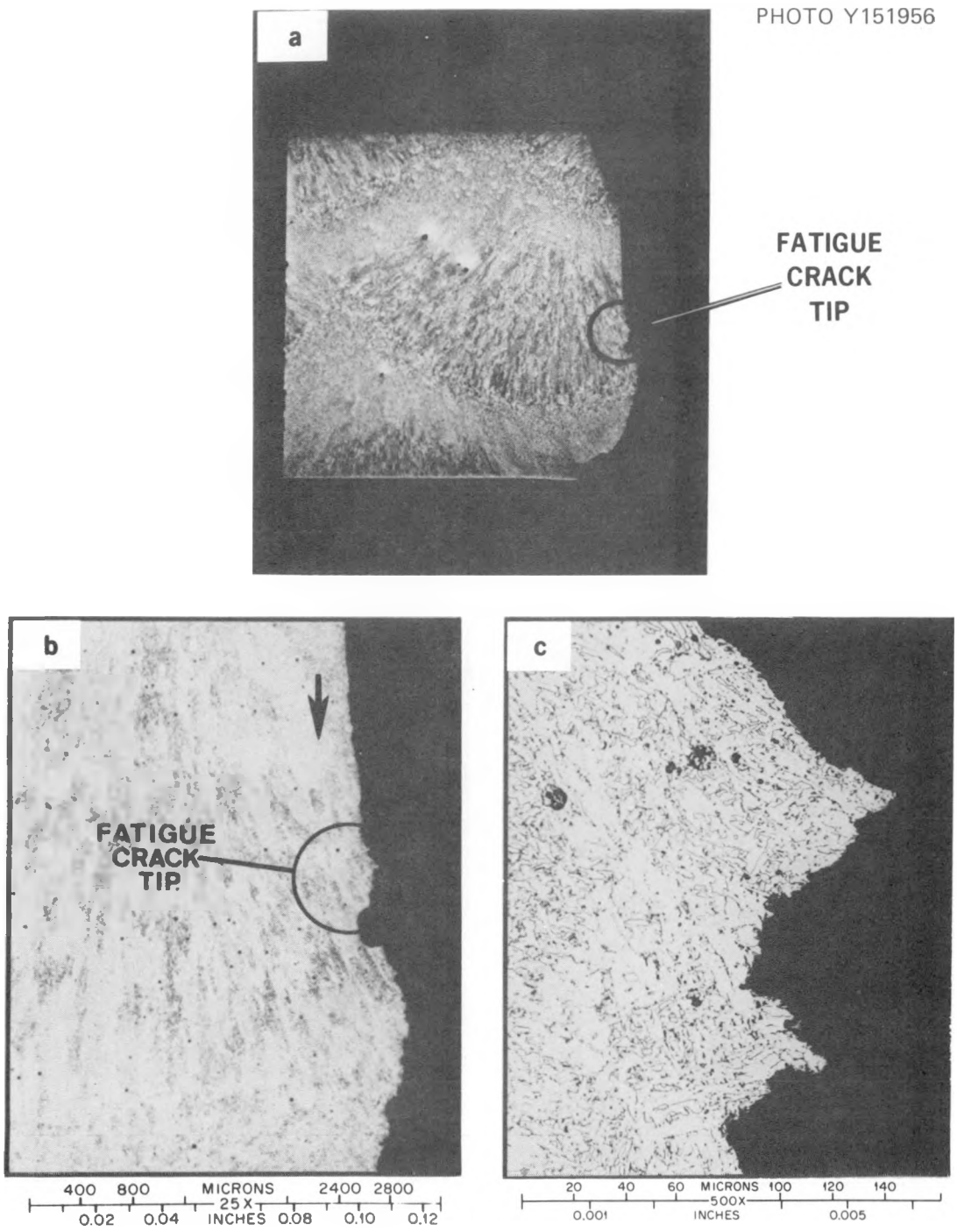

Fig. 5.13. Metallographic examination of the crack tip region of PCC_V specimen V8W74. This specimen was tested at −18°C and exhibited a K_{Icd} toughness value of 225 $MN \cdot m^{-3/2}$. The crack tip resides in the coarse columnar-grained region of the weld metal. This can be seen in (*a*) and (*b*); (*c*) is a photomicrograph of the microstructure at the crack initiation site. Original reduced 11%.

weld passes by the subsequent passes. The weld metal contains regions of as-deposited and, when postweld heat treated, tempered microstructures. These are regions that contain coarse columnar grains. The brittle-to-ductile transition temperature of this microstructure is higher than that of the weld metal regions that are reaustenitized due to subsequent weld passes. The columnar grains in these reaustenitized regions are refined, thereby resulting in a microstructure with considerably superior toughness properties. These differences in properties are reflected in the toughness exhibited by the PCC_V specimens tested in a temperature regime where this difference occurs. At low temperatures, −73°C, all the microstructures are brittle and the weld metal exhibits frangible behavior regardless of the location of the fatigue crack tip. Consequently, the spread in toughness values obtained for the weld metal is reduced. A similar phenomenon occurs at elevated temperatures. All microstructures are above their transition temperatures at −18°C, and once again the spread in toughness values is reduced. The location of the crack tip is important only in the temperature regime where the various microstructures in the weld metal exhibit variable toughness properties.

5.3 Crack-Arrest Model Studies

W. J. Stelzman D. A. Canonico

5.3.1 Material characterization for small crack-arrest models

The characterization of the "quenched-and-tempered" W57 base plate and the "quenched-only" plate 03JZ used in the crack-arrest model tests[6] has continued. Static fracture toughness (K_{Icd}) results from RT-oriented 0.394T (C_VT) and 1T compact specimens are presented in Table 5.3 together with results from the C_VT compact specimens reported previously.[4] The compact specimen results, where comparable, agree very well with the static fracture toughness results from precracked Charpy specimens.

Table 5.3. Static fracture toughness results from compact specimens of as-quenched 03JZ and W57 base plate

Specimen type	Depth[a] t	Depth[a] T	Orientation	Test temp. (°C)	K_{Icd} ($MN \cdot m^{-3/2}$)
As-quenched plate 03JZ					
1T	0.5	0.3	RT	4.4	140
1T	0.5	0.7	RT	−45.6	97
0.394T	0.3	0.4	RT	−101	65
0.394T	0.7	0.4	RT	−20.6	133
W57 base plate					
1T		0.4	RT	−45.6	165
1T		0.6	RT	−73.3	102
0.394T		0.4	RT	−45.6	115
0.394T		0.6	RT	−73.3	91
0.394T		0.5	RT	−129	55

[a] See Ref. 7 for definition of depths.

References

1. P. P. Holz, "Preparations for HSST Intermediate Vessel Tests V-7B and V-8," *Heavy-Section Steel Technology Program Quart. Prog. Rep. October–December 1976*, ORNL/NUREG/TM-94, pp. 32–38.
2. R. H. Bryan, "Pressure Vessel Investigations," *Heavy-Section Steel Technology Program Quart. Prog. Rep. July–September 1977*, ORNL/NUREG/TM-166.
3. R. W. Derby et al., *Test of 6-inch-thick Pressure Vessels. Series 1: Intermediate Test Vessels V-1 and V-2*, ORNL-4895 (February 1974).
4. W. J. Stelzman and D. A. Canonico, "Characterization of the Repair Weld in Vessel V-8," *Heavy-Section Steel Technology Program Quart. Prog. Rep. July–September 1977*, ORNL/NUREG/TM-166.
5. W. J. Stelzman and D. A. Canonico, "Characterization of the V-7B and V-8 Repair Weldments," *Heavy-Section Steel Technology Program Quart. Prog. Rep. January–March 1977*, ORNL/NUREG/TM-120, pp. 40–44.
6. G. C. Smith, "Third Crack-Arrest Model Test," *Heavy-Section Steel Technology Program Quart. Prog. Rep. April–June 1977*, ORNL/NUREG/TM-147.
7. W. J. Stelzman and D. A. Canonico, "Material Tests for Small Crack-Arrest Test Vessels," *Heavy-Section Steel Technology Program Quart. Prog. Rep. October–December 1976*, ORNL/NUREG/TM-94, pp. 51–58.

6. THERMAL SHOCK INVESTIGATIONS*

R. D. Cheverton S. E. Bolt

6.1 Introduction

During this reporting period for the LOCA-ECC Thermal Shock Program, construction of the liquid-nitrogen thermal shock test facility (LN_2-TSTF) was completed, shakedown runs with water and LN_2 were conducted, a new method for applying the LN_2 heat transfer enhancement coating was developed, heat transfer coefficients associated with the new coating were determined in small-scale LN_2 quench experiments, and the new three-dimensional, finite-element, linear elastic fracture mechanics (LEFM) code was completed.

6.2 Cryogenic Test Facility for 533-mm-OD Test Specimens

Construction of the liquid-nitrogen thermal shock test facility (LN_2-TSTF) was completed, and shakedown tests were conducted with the TSV-F test specimen, first using water as the heat sink and then liquid nitrogen. Following these preliminary tests, a few modifications were made to the facility and to operating procedures. The present version of the facility is shown in Fig. 6.1, and a discussion of how the facility imposes a thermal shock on the 533-mm-OD test specimen is found in Ref. 1.

6.3 Heat Transfer to Liquid Nitrogen

When liquid nitrogen comes in contact with a relatively hot metal surface, a nitrogen vapor blanket forms (film boiling regime) that "insulates" the surface and prevents a rapid quench. This situation can be circumvented by applying a thin coating of a solid insulating material to the metal surface. This insulating coating initially reduces the surface

---

*Conversions from SI to English units for all SI quantities are listed on a foldout page at the end of this report.

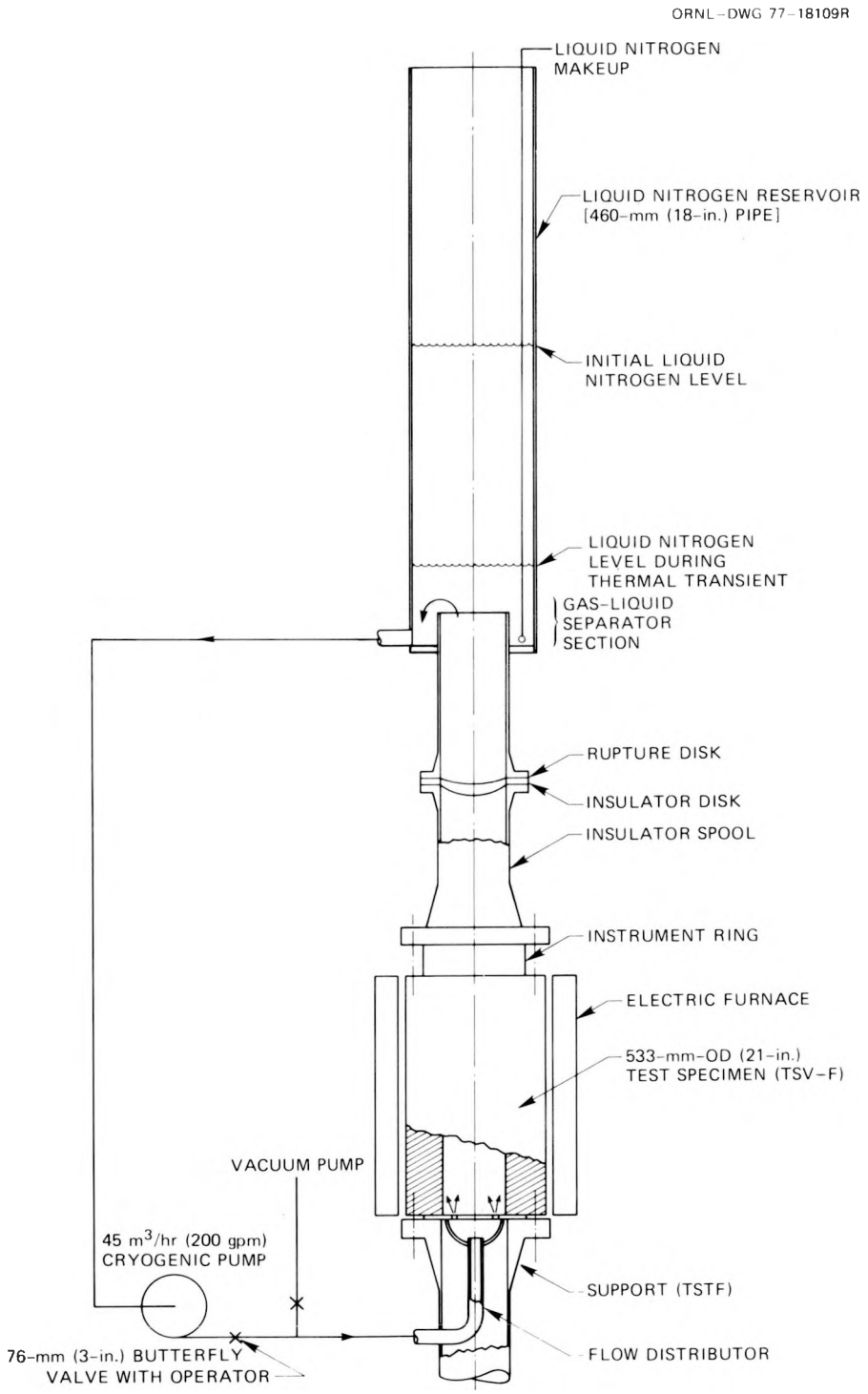

Fig. 6.1. Liquid-nitrogen thermal shock test facility.

heat flux and thus the temperature drop across the nitrogen fluid film and allows the nucleate boiling regime to be established. The heat transfer coefficient for this regime is much greater than that for film boiling.

A further enhancement in heat transfer coefficient can be achieved by increasing the number of nucleation sites on the surface of the insulating coating. In recent months we have used 3M-brand Spray Adhesive 77 as the insulating material and have achieved a high density of nucleation sites under appropriate spraying conditions. Results obtained from LN_2-quench heat transfer tests[1-3] on small cylinders indicate that adequate heat transfer coefficients for proposed thermal shock experiments (see Ref. 1) can be achieved.

In preparation for the heat transfer experiments, the Spray Adhesive 77 coating was applied by means of a spray can, and the distance from nozzle to metal surface was found to be critical in terms of achieving a high density of nucleation sites (the droplet must dry to a certain extent while in flight). Because of the small internal diameter and greater length of the TSV-F test specimen (241 mm ID × 914 mm length), it is not possible to spray the interior of the latter specimen in the manner used for the shorter specimens. After conferring with 3M personnel, we decided to use a nearly conventional "paint" spray gun with a somewhat different adhesive material, 3M-brand NF-34, which could be obtained in bulk.

During spray-technique development tests, the modified gun was attached to a mandrel that guided the gun along the longitudinal centerline of a 250-mm pipe test specimen 910 mm long. The nominal spray direction was along the centerline of the pipe so that the path from nozzle to pipe inner surface was a diagonal, as illustrated in Fig. 6.2. The length of the diagonal can be varied by adjusting the nozzle air flow. The spray pattern is fan shaped, and thus it is necessary to rotate the pipe while withdrawing the gun in order to obtain a uniform coat.

Once a reasonable adhesive flow rate and spray pattern were achieved using a stationary target, the inner surface of the 250-mm pipe was sprayed. A 300-mm length of the pipe was removable from the far end; following spray application and a several-hour drying period, the removable section was insulated on the outer surface and the unit quenched

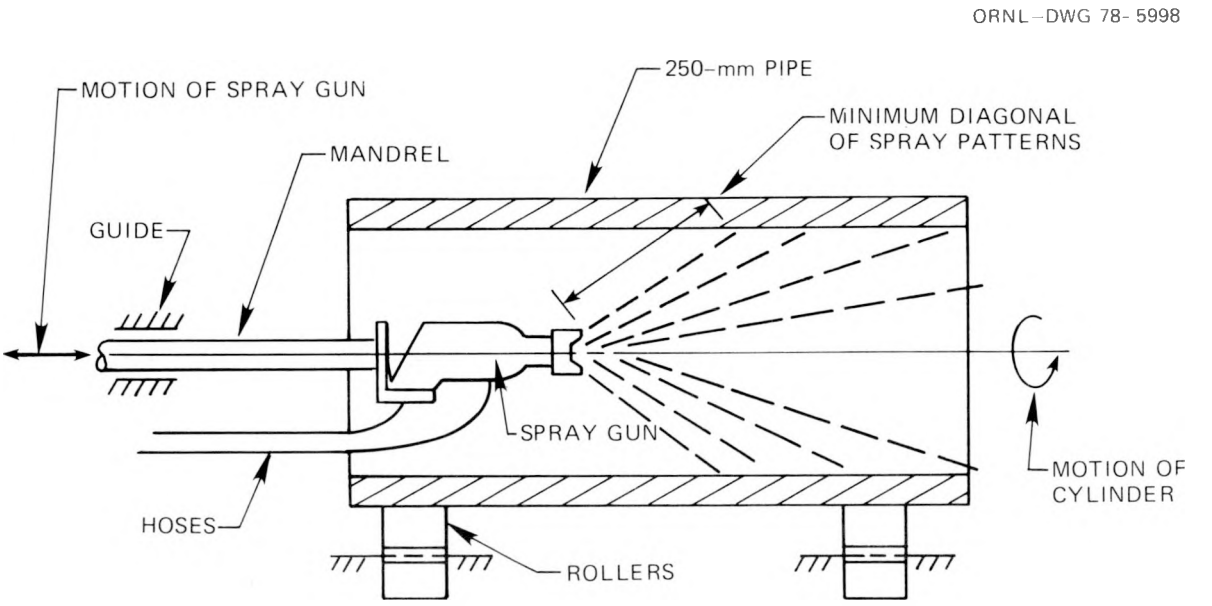

Fig. 6.2. Horizontal spray facility.

in LN_2 by submergence. The quench rate was recorded by means of thermocouples embedded in the wall. The specimen was quenched first from room temperature and then from 93°C. Following these two quenches, the specimen was again assembled to the remaining 610-mm length of pipe and a second coating applied. Two thermal shocks were administered to the 300-mm length of pipe as before, followed by application of a third coat and then two more thermal shocks. The successive tests were conducted in an effort to establish the optimum coating thickness. The tests were similar to experiments conducted earlier and discussed in Refs. 2 and 3.

Results of the above experiments are shown in Figs. 6.3 and 6.4 in terms of wall temperature vs time for a particular radial location in the wall, and in Figs. 6.5 and 6.6 in terms of heat transfer coefficient vs metal surface temperature, where the coefficient includes the resistance of the coating. Figure 6.6 shows a comparison between heat transfer coefficients obtained earlier using the Spray Adhesive 77 coating on a different specimen* and coefficients obtained using the latest technique

*The initial temperature of the specimen was 93°C (200°F). This curve was used in feasibility studies for a cryogenic quench of the 39-in.-OD test specimen with an initial temperature of 93°C (200°F) (see Ref. 1).

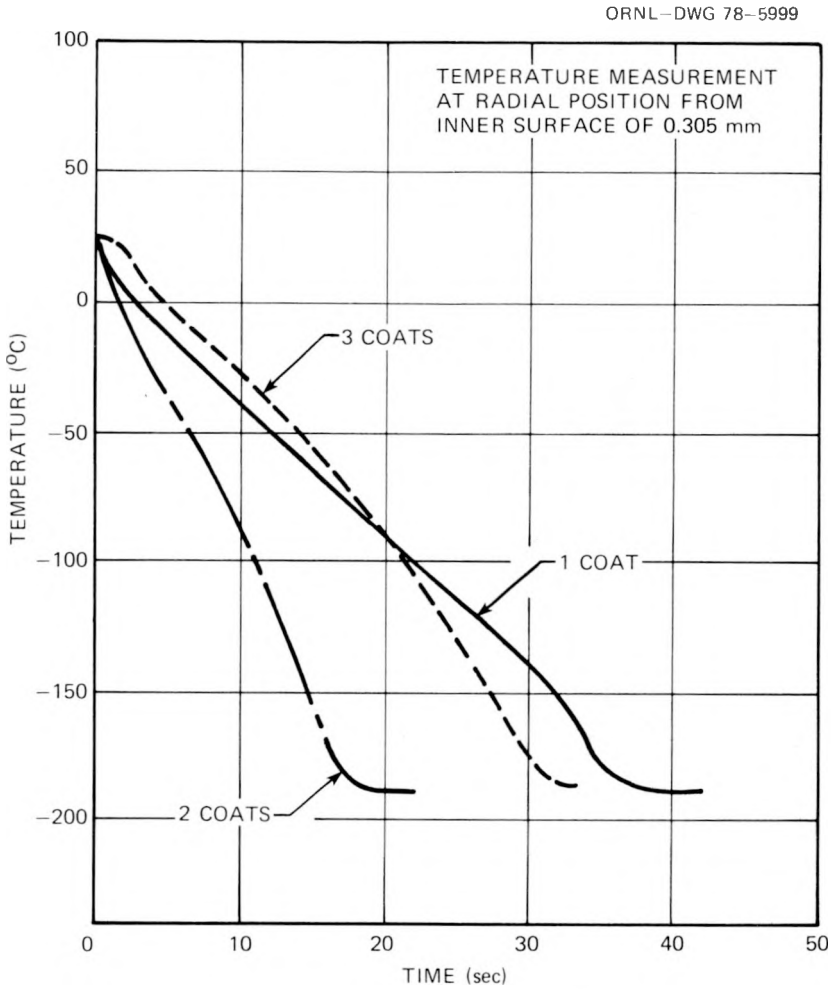

Fig. 6.3. Temperature transient during LN_2 quench of 250-mm-ID, 9.40-mm-wall, 300-mm-long test specimen insulated on outer surface and coated on inner surface with different thicknesses of 3M-brand NF-34. Initial temperature ∿24°C.

on the 250-mm pipe. It is observed that the latest coating technique results in a higher coefficient. Thus, this technique is adequate for the proposed thermal shock experiments so far as we know.

Figures 6.5 and 6.6 indicate relatively low values of the heat transfer coefficient at the outset of the thermal shock. It is believed that this is associated with the finite time for submergence of the test specimen. At least in the range 24 to 93°C, the low values are not associated with a specific initial metal surface temperature, as indicated by a comparison of Figs. 6.5 and 6.6.

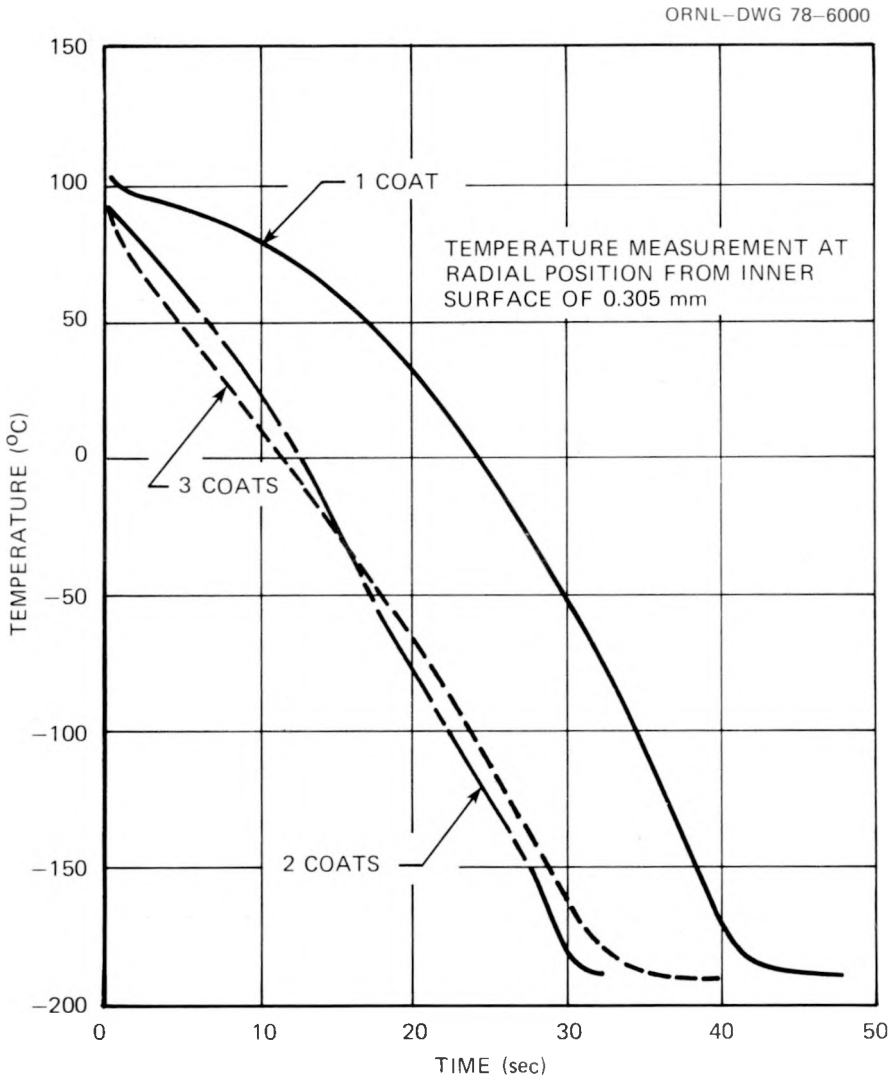

Fig. 6.4. Temperature transient during LN_2 quench of 250-mm-ID, 9.40-mm-wall, 300-mm-long test specimen insulated on outer surface and coated on inner surface with different thicknesses of 3M-brand NF-34. Initial temperature ∿93°C.

The surface texture of the NF-34 coating is quite rough, a condition that contributes to a high density of nucleation sites but that makes accurate measurement of effective coating thickness very difficult. Estimates of coating thickness obtained using a magnetic device (Mikrotest Nordson Corp.) and an eddy-current device (Kaman Multi-Vit model KD-2300-2S) are shown in Table 6.1. For both instruments the measurements

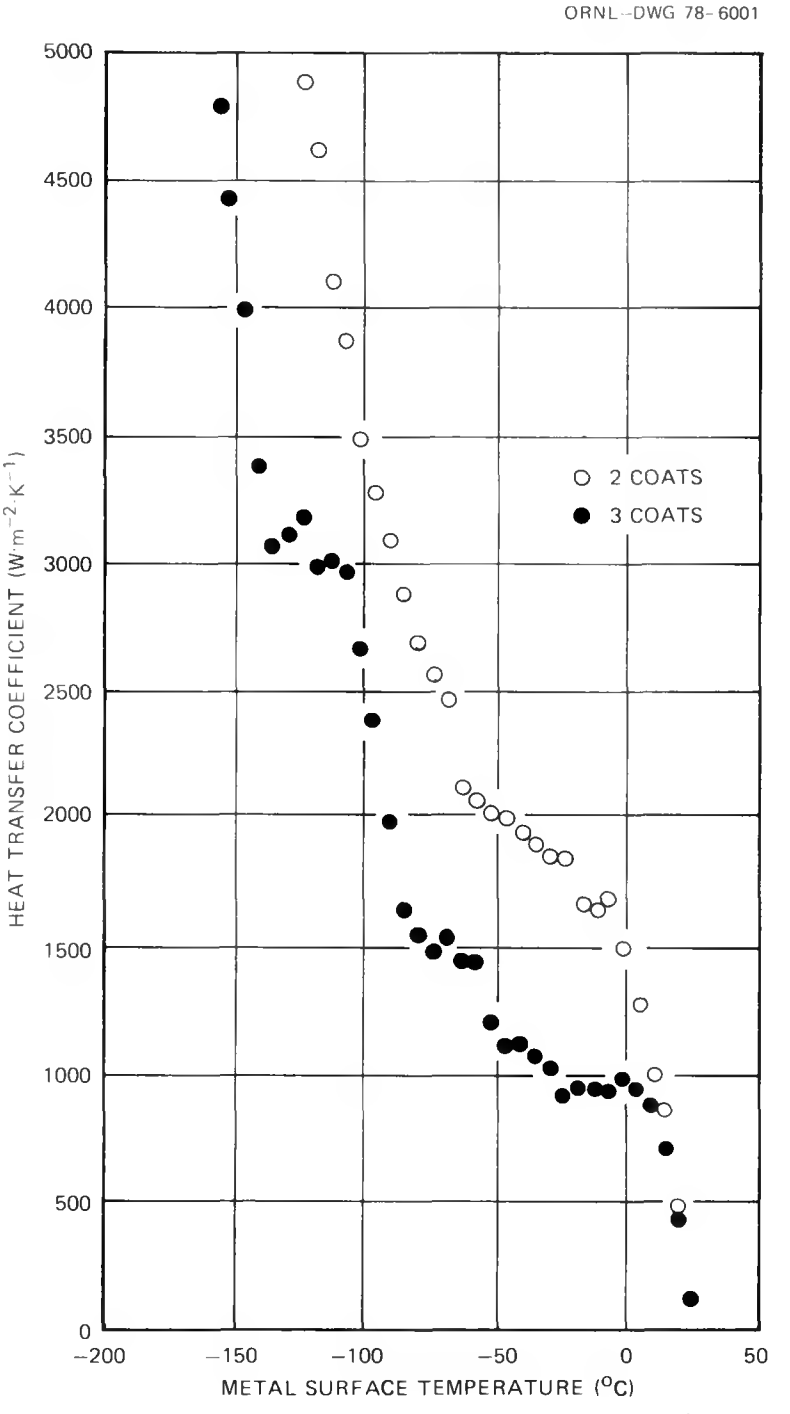

Fig. 6.5. Heat transfer coefficient vs metal surface temperature during LN_2 quench of 250-mm-ID, 9.40-mm-wall, 300-mm-long test specimen insulated on outer surface and coated on inner surface with different thicknesses of 3M-brand NF-34. Initial temperature ∿24°C.

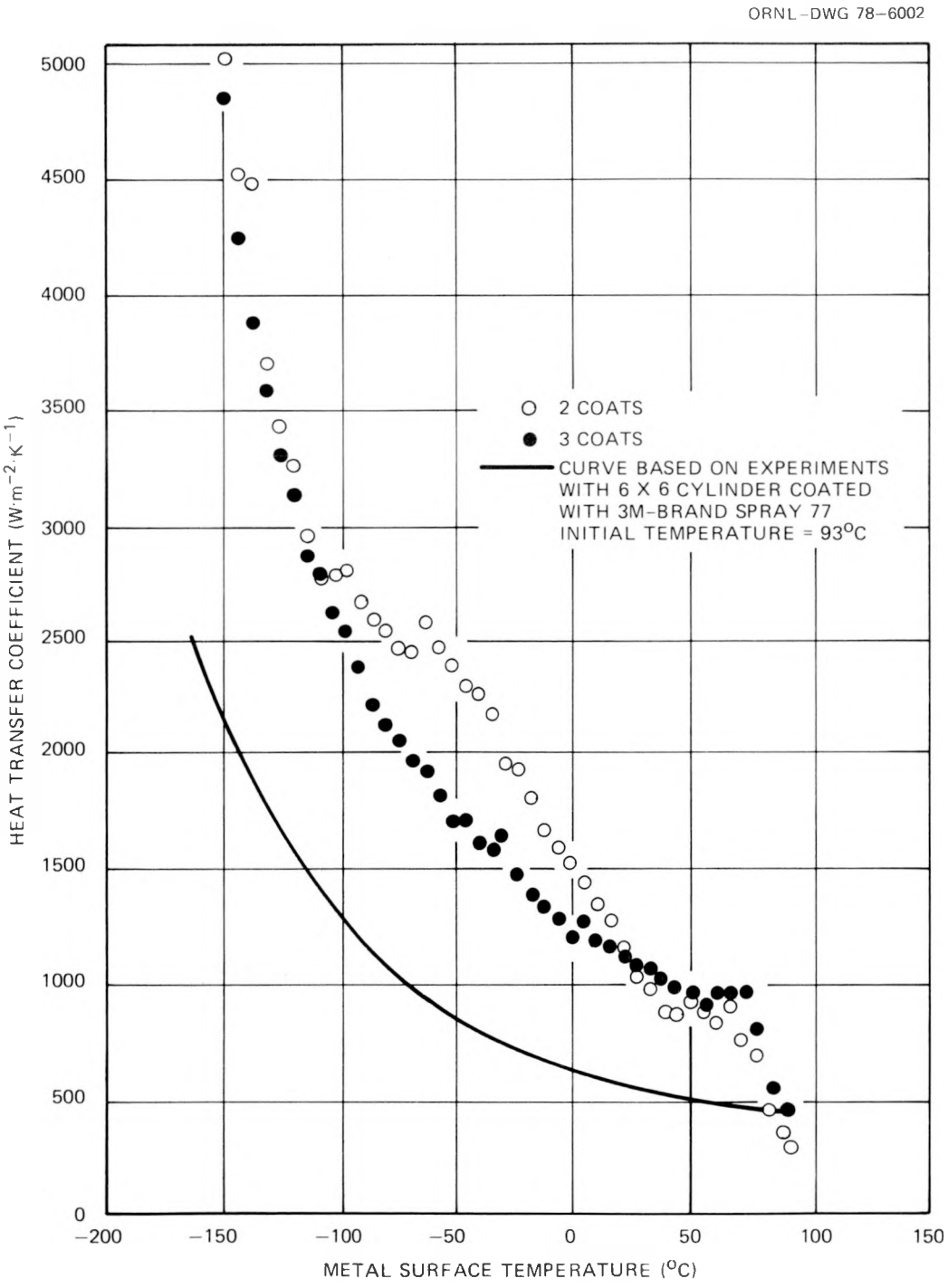

Fig. 6.6. Heat transfer coefficient vs metal surface temperature during LN_2 quench of 250-mm-ID, 9.40-mm-wall, 300-mm-long test specimen insulated on outer surface and coated on inner surface with different thicknesses of 3M-brand NF-34. Initial temperature ∿93°C.

Table 6.1. NF-34 coating thickness on inner surface of 250-mm-pipe coating-development test specimen

Coating No.	Measuring device	Indicated thickness[a] (mm)
1. (11-28-77, 11-29-77)	Magnetic	0.30,[b] 0.28[c]
2. (11-30-77)	Eddy current	0.43[c]
3. (11-31-77)	Eddy current	0.56,[b] 0.56[c]

[a]Average of 27 readings from vicinity of thermocouple locations. Magnetic readings varied ±25%, while eddy-current readings varied ±6%.

[b]Prior to quench.

[c]Following 93°C quench.

are sensitive to pressure applied to the hand-held transducer because the roughness of the coating tends to flatten under mechanical pressure. Furthermore, the stylus of the magnetic device may fall on top of or between the peaks. Because of this latter situation the eddy-current device is preferred. This instrument appears to be adequate because it is only necessary that consistent relative measurements be made in order to achieve the desired coating thickness on the fracture mechanics test specimen.

The spray facility used in these initial development tests restricted the position of the test specimen to a horizontal orientation and is not suitable for spraying the full length of TSV-F. A new facility was constructed that rotates the specimen about a vertical centerline, as shown in Fig. 6.7.

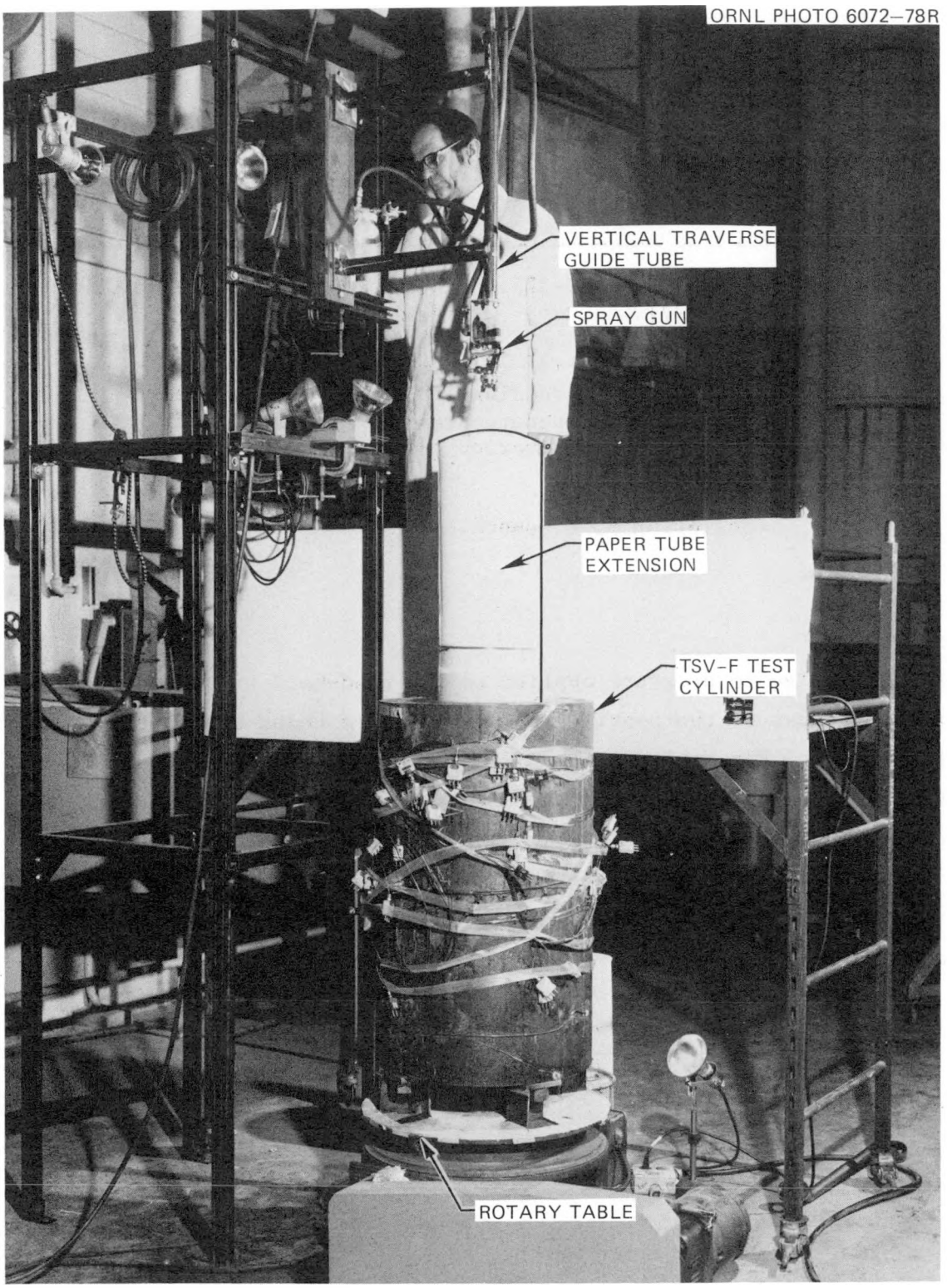

Fig. 6.7. Photograph of the vertical spray facility used for coating the inner surface of the 533-mm-OD test specimen.

References

1. R. D. Cheverton, "Thermal Shock Investigations," *Heavy-Section Steel Technology Program Quart. Prog. Rep. July–September 1977*, ORNL/NUREG/TM-166.

2. R. D. Cheverton, "Thermal Shock Investigations," *Heavy-Section Steel Technology Program Quart. Prog. Rep. January–March 1977*, ORNL/NUREG/TM-120, pp. 73–101.

3. R. D. Cheverton, "Thermal Shock Investigations," *Heavy-Section Steel Technology Program Quart. Prog. Rep. April–June 1977*, ORNL/NUREG/TM-147, pp. 69–89.

7. FOREIGN RESEARCH

W. L. Greenstreet

The objective of this task is to systematically collect, maintain, and review products of foreign research that are applicable to safety of LWR primary systems. The areas to be covered are fracture mechanics, metallurgy, welding, and structures fabrication. The validity and usefulness of foreign results for application to safety and licensing of LWRs are to be identified to NRC, and recommendations are to be made concerning the application of pertinent well-founded research results.

Lists of foreign reports published in *Nuclear Safety* through Vol. 19 (No. 1) (January–February 1978) have been reviewed to identify topics of interest in the metallurgy and materials areas. A total of 21 foreign language research reports have been identified, and requests for translated copies have been submitted to NRC. Six translated documents, plus two which were not on the request lists, have been received. These documents are being reviewed as they become available.

CONVERSION FACTORS[a]

SI unit	English unit	Factor
mm	in.	0.0393701
kPa	psi	0.145038
MPa	ksi	0.145038
$MN \cdot m^{-3/2}$ ($MPa \cdot \sqrt{m}$)	$ksi\sqrt{in.}$	0.910048
J	ft-lb	0.737562
K	°F or °R	1.8
kJ/m^2	$in\text{-}lb/in.^2$	5.71015
$W \cdot m^{-2} \cdot K^{-1}$	$Btu/hr\text{-}ft^2\text{-}°F$	0.176110
$T(°F) = 1.8\ T(°C) + 32$		

[a]Multiply SI quantity by given factor to obtain English quantity.

ORNL/NUREG/TM-194
Dist. Category NRC-5

Internal Distribution

1. R. G. Berggren
2. S. E. Bolt
3. R. H. Bryan
4. J. H. Butler
5. J. P. Callahan
6. D. A. Canonico
7. S. J. Chang
8. R. D. Cheverton
9. W. E. Cooper
10. J. M. Corum
11. W. B. Cottrell
12. M. H. Fontana
13. W. R. Gall
14. W. L. Greenstreet
15. R. C. Gwaltney
16. J. F. Harvey
17. M. R. Hill
18. P. P. Holz
19. H. W. Hoffman
20. S. K. Iskander
21. M. A. Karnitz
22. K. K. Klindt
23. Milton Levenson
24. R. E. MacPherson
25. R. W. McClung
26. J. R. McGuffey
27. J. G. Merkle
28. C. A. Mills
29. S. E. Moore
30. F. R. Mynatt
31. F. H. Neill
32. H. A. Pohto (Y-12)
33. G. C. Robinson
34. C. D. St. Onge (Y-12)
35-36. Myrtleen Sheldon
37. G. M. Slaughter
38. C. B. Smith
39. G. C. Smith
40. J. E. Smith
41. I. Spiewak
42. W. J. Stelzman
43. D. G. Thomas
44. H. E. Trammell
45. J. R. Weir, Jr.
46-99. G. D. Whitman
100. Patent Office
101-102. Central Research Library
103. Y-12 Document Reference Section
104-108. Laboratory Records Department
109. Laboratory Records, RC

External Distribution

110-117. Director, Office of Nuclear Regulatory Research, Nuclear Regulatory Commission, Washington, D.C. 20555
118. Director, Reactor Division, Department of Energy, Oak Ridge Operations Office
119. Director, Research and Technical Support Division, Department of Energy, Oak Ridge Operations Office
120-287. Special HSST Distribution
288-662. Given distribution under category NRC-5 (25 copies — NTIS)

☆ U.S. GOVERNMENT PRINTING OFFICE: 1978-748-189/36